

# A multi-disciplinary analysis of the exceptional flood event of July 2021 in central Europe. Part 2: Historical context and relation to climate change

Patrick Ludwig<sup>1,2</sup>, Florian Ehmele<sup>2</sup>, Mário J. Franca<sup>3</sup>, Susanna Mohr<sup>1,2</sup>, Alberto Caldas-Alvarez<sup>2</sup>, James E. Daniell<sup>1,4</sup>, Uwe Ehret<sup>1,3</sup>, Hendrik Feldmann<sup>2</sup>, Marie Hundhausen<sup>2</sup>, Peter Knippertz<sup>2</sup>, Katharina Küpfer<sup>1,2</sup>, Michael Kunz<sup>1,2</sup>, Bernhard Mühr<sup>1</sup>, Joaquim G. Pinto<sup>1,2</sup>, Julian Quinting<sup>2</sup>, Andreas M. Schäfer<sup>1,5</sup>, Frank Seidel<sup>3</sup>, and Christina Wisotzky<sup>1,6</sup>

<sup>1</sup>Center for Disaster Management and Risk Reduction Technology (CEDIM), Karlsruhe Institute of Technology (KIT), Karlsruhe, Germany

<sup>2</sup>Institute of Meteorology and Climate Research, Karlsruhe Institute of Technology (KIT), Karlsruhe, Germany

<sup>3</sup>Institute for Water and River Basin Management, Karlsruhe Institute of Technology (KIT), Karlsruhe, Germany

<sup>4</sup>Institute of Photogrammetry and Remote Sensing, Karlsruhe Institute of Technology (KIT), Karlsruhe, Germany

<sup>5</sup>Geophysical Institute, Karlsruhe Institute of Technology (KIT), Karlsruhe, Germany

<sup>6</sup>Institute of Economics, Karlsruhe Institute of Technology (KIT), Karlsruhe, Germany

**Correspondence:** Patrick Ludwig (patrick.ludwig@kit.edu)

**Abstract.** Heavy precipitation over western Germany and neighboring countries in July 2021 led to widespread floods, with the Ahr and Erft river catchments being particularly affected. Following the event characterization and process analysis in Part 1, here we put the 2021 event in the historical context regarding precipitation and discharge records, and in terms of the temporal transformation of the valley morphology. Furthermore, we evaluated the role of ongoing and future climate change 5 on the modification of rainfall totals and **associated flood hazards** **the associated flood hazard** as well as implications for flood management.

The event was among the five heaviest precipitation events of the past 70 years in Germany. However, considering the large LAERTES-EU regional climate model (RCM) ensemble revealed a substantial underestimation of **return values** **both return levels** and periods based on extreme value statistics using only observations. An analysis of homogeneous hydrological 10 data of the last 70 years demonstrated that the event discharges exceeded by far the statistical 100-year return **values** **levels**. Nevertheless, the flood peaks at the Ahr River were comparable to the reconstructed major historical events of 1804 and 1910, which were not included in the **hazard assessment of flood risk** **flood risk assessment** so far. A comparison between the 2021 and past events showed differences in terms of the observed hydro-morphodynamic processes which enhanced the flood risk due to changes in the landscape organization and occupation.

15 The role of climate change and how the 2021 event would unfold under warmer or colder conditions (within a  $-2\text{ K}$  to  $+4\text{ K}$  range) was **analyzed based on** **considered based on** **both a** pseudo-global-warming (PGW) model experiments. **These and the analysis of an RCM ensemble**. **The PGW experiments** showed that the spatial mean precipitation scales **to first order** with the theoretical Clausius-Clapeyron (CC) relation, predicting a 7 to 9 % increase per degree **of** warming. Using the PGW rainfall simulations as input to a hydrological model of the Ahr river basin revealed a strong and non-linear effect on flood peaks: For

20 the +2 K scenario, the 18 % increase in areal rainfall led to a 39 % increase of the flood peak at gauge Altenahr. The analysis of the high-resolution convection-permitting KIT-KLIWA RCM ensemble confirmed the CC-scaling for moderate spatial mean precipitation but showed a super CC-scaling of up to 10 % for higher intensities. Moreover, also the spatial extent of such precipitation events is expected to increase.

## 1 Introduction

25 In mid-July 2021, heavy precipitation over two days exceeding 150 mm affected a large area covering western Germany with the adjacent regions in the Netherlands, Belgium, Luxembourg, and France, triggering widespread flooding (e.g., Schäfer et al., 2021; Junghänel et al., 2021; Dewals et al., 2021; MeteoLux, 2021). Especially areas in the German federal states of North-Rhine Westphalia (NRW) and Rhineland-Palatinate (RP), Luxembourg, and eastern Belgium were heavily affected by floods, in particular, the river catchments of the Ahr and Erft (Fig. 1a). The area of these two is characterized by the low mountain ranges 30 of the Eifel and the Ardennes. Both the Ahr and the Erft Rivers are tributaries of the Rhine River, the former with a catchment area of approx. 900 km<sup>2</sup>, and the latter with approx. 1800 km<sup>2</sup>. On 14 July 2021, precipitation totals widespread reached values of more than 75 mm in 24 hours (locally even over 100 mm; Fig. 1b) with most of the precipitation even falling within 15 hours (Mohr et al., 2022). Severe damage to buildings, infrastructure, and industry as well as the loss of over 180 lives 200 lives (Tradowsky et al., 2022) with more than 180 fatalities in Germany alone (Kreienkamp et al., 2021) was the result. The event 35 was one of the five costliest disasters in Europe in the last half-century 50 years (Mohr et al., 2022), with Munich Re (2022) estimating a total loss of 46 billion Euros and 33 billion Euros in Germany alone. Even one year later, reconstruction work is still ongoing, and it will take years until all infrastructure is back in place (BMDV, 2021, 2022).

This two-part interdisciplinary study emerged from activities (Sehäuser et al., 2021) within the Center for Disaster Management and Risk Reduction Technology (CEDIM; ; last access: 9 May 2022), an interdisciplinary research center in 40 the field of disasters, risks, and security at the Karlsruhe Institute of Technology (KIT), Germany. CEDIM conducts so-called Forensic Disaster Analyses (FDA) in near-real time since 2011 (e.g., Kunz et al., 2013; Merz et al., 2014; Piper et al., 2016; Wilhelm et al., 2021) aiming to get an overview of a disaster including identification of main drivers and assessing related impacts within a few hours to days after the event. The first part of 45 this study (Mohr et al., 2022, hereafter referred to as PART1) (Mohr et al., 2022, hereafter referred to as PART 1) focused on the characterization and analysis of the event itself encompassing the interlink of meteorological, hydrological, and hydro-morphological processes and effects. In addition, the extension of the inundation areas and impacts like traffic disruption and economic losses were addressed.

The synoptic large-scale conditions that led to the heavy precipitation event were characterized by a quasi-stationary, large-scale trough and an associated low-pressure system over the region, which was sustained by a blocking event over the eastern 50 North Atlantic. These synoptic patterns were well predicted by the numerical weather prediction models operated by Deutscher Wetterdienst (DWD) or the European Centre for Medium-Range Weather Forecasts (ECMWF). Such large-scale situations foster extreme weather events like the one discussed here (e.g., Woollings et al., 2018; Kautz et al., 2022). The predicted

and observed rainfall totals were extreme for that particular region exceeding high return periods affecting an uncommonly large area (cf. PART1). The PART 1). Likewise, the recorded and reconstructed flood peaks were extraordinary and were 55 exacerbated by the morphological characteristics of the catchments and river channel network, and by the landscape occupation and organization, both. Both aspects were responsible for widespread inundation of the valley, the generalized occurrence of erosion and scouring processes, deposition, clogging, and damming of channel network bottlenecks such as bridges, streets, and narrow river sections, or eventually the collapse of the structure of the channel network with the observation of flow bypasses and riverbank collapses.

60 A key aspect that needs deeper analysis is the evaluation is a deeper analysis of the 2021 flood event from based on a long-term climatological perspective. For example, the Ahr catchment had been affected by two severe flood events in 1804 and 1910 (Roggenkamp and Herget, 2014a, b). In spite of the limited data available, evidence is given that these events might have been the 1804 event was comparable to the July 2021 event in terms of discharge (PART1; Roggenkamp and Herget, 2022) peak discharge (PART 1; Roggenkamp and Herget, 2022). However, these events were not considered for the official estimation of 65 the 100-year return periods of discharge ( $HQ_{100}$ ) by the Landesamt für Umwelt (LfU) of RP as the continuous time series of observations only starts in 1946. Thus, Vorogushyn et al. (2022) recently estimated the return period of the 2021 flood at gauge Altenahr (Ahr) based only on the recorded data from 1946 to 2019 to be more than  $10^8$  years, which is very unrealistic and clearly shows the limits of the extreme value statistics for rare events. In contrast, taking into account reconstructed 70 historical floods since 1804, the return period of the 2021 flood is reduced to an order of magnitude of  $HQ_{10000}$ . In addition, the consequences such as inundation areas and depths in the valley during the past and the 2021 floods differ dramatically in some cases. This can also be attributed to changes in the landscape or in landscape use and newly emerging process connections and 75 feedbacks (cf. PART1; Dietze et al., 2022)(cf. PART 1; Dietze et al., 2022).

Because the dimensions of the July 2021 event were somehow surprising and unexpected, the role of ongoing and future climate change (IPCC, 2022)(IPCC, 2021a, 2022) on the evolution and characteristics of such extreme events is an 80 important issue to be addressed. According to the Clausius-Clapeyron (CC) relationship, the intensity and probability of precipitation events are affected by an increase in moisture content of 7% per degree temperature increase (e.g., Allen and Ingram, 2002; Pall et al., 2007). In fact, on the global scale, the general circulation models (GCMs) project an increase in heavy precipitation over large areas of the globe which, however, scales not necessarily with the CC-rate (Stoecker, 2014; ?) (magnitude varies between 4% and 8% per 1K of surface warming; IPCC, 2021a). One possible reason is the resolution of 85 GCMs (usually 100 to 200 km) used for the future projections (ScenarioMIP; usually 80 to 250 km; IPCC, 2021b), which is too coarse to fully capture the local characteristics and intensities of (heavy) precipitation events contributing to the total amounts. A possible approach to overcome this shortcoming is the consideration of regional climate model (RCM) simulations with typical horizontal resolutions of 12 to 25 km or even down to convection-permitting resolutions below 3 km (e.g., Vergara-Temprado et al., 2021). A good overview of the advantages of large RCM ensembles is given in Maher et al. (2021). 90 For example, for the historical period, the LAERTES-EU data set (Ehmele et al., 2020, 2022) with over 12 000 years at 25 km horizontal resolution provides an excellent basis to estimate how uncommon precipitation values are in the scope of recent climate conditions. Moreover, the examination of convection-permitting ensemble simulations (Prein et al., 2015; Ban et al.,

2021) further improves the basis for such an evaluation, given that such models exhibit a largely reduced bias in terms of precipitation intensities compared to lower resolution (12 to 25 km) climate models (Prein et al., 2015; Caldas-Alvarez et al., 90 2022b).

While conventional climate model simulations are used to assess the general evolution of precipitation characteristics, so-called attribution studies elaborate on how climate change affects specific events. Such studies consider a very large number of climate model simulations with and without anthropogenic forcing (probabilistic event attribution). By comparing the statistics of both types of simulation, it is possible to estimate whether the probability of occurrence of a specific event has changed in recent decades or not (Allen and Ingram, 2002; Stott et al., 2004, 2016; Otto, 2017). Furthermore, climate model simulations can 95 also be used for conditional event attribution investigations as an alternative complementary to the above-described probabilistic approach (Stott et al., 2016). The conditional approach is often referred to as the “storyline” approach (e.g., Shepherd, 2016; Shepherd et al., 2018; Shepherd, 2019), which assesses the extent to which recent climate change and future projected conditions could affect the magnitude of a specified event

100 (e.g., Trenberth et al., 2015; Sillmann et al., 2021; Sánchez-Benítez et al., 2022) by performing coupled climate model simulations specific historical event (e.g., Trenberth et al., 2015; Sillmann et al., 2021; Sánchez-Benítez et al., 2022). The storyline approach can be useful to individually investigate the thermodynamic (e.g., increase in moisture) and the dynamic component (changes in atmospheric circulation) for a specific event. As stated by Shepherd (2016), the thermodynamic aspects of climate change are generally robust in theory and their impacts, particularly on precipitation, can thus be studied by keeping

105 the dynamics constant e.g., by spectral nudging (van Garderen et al., 2021). A variant of this approach is to assess climate change and its impact on extreme events with a pseudo-global-warming (PGW) analysis (e.g., Schär et al., 1996; Michaelis et al., 2017). In this case, the thermodynamic modifications are imprinted to the initial and lateral boundary forcing data of RCM simulations, such as temperature changes corresponding to a fixed warming level (e.g., +2 K) or by considering the mean changes from the background environmental conditions from GCMs under a given scenario (e.g., Aalbers et al., 2022).

110 For the July 2021 event, a study from the World Weather Attribution initiative (e.g., Otto, 2017) estimated an increase in the probability of occurrence already by a factor between 1.2 and 9 compared to a 1.2 K colder climate (Kreienkamp et al., 2021) (Kreienkamp et al., 2021; Tradowsky et al., 2022). Examples of similar work have already been performed for other severe flood events (e.g., Lackmann, 2013; Lenderink et al., 2021).

115 In the present study (hereafter referred to as PART2PART 2), we put the July 2021 event into a historical context using both observational and the LAERTES-EU data sets. Regarding climate change, we consider an ensemble of convection-permitting climate simulations and novel PGW simulations that were performed specifically for this event. The following research questions are addressed:

- (I) How does the event classify within the historical context of precipitation and flood events?
- (II) In which way did the historical transformation of river valleys (e.g., landscape occupation and organization) change the 120 2021 flood hazard in comparison to past events in this region?

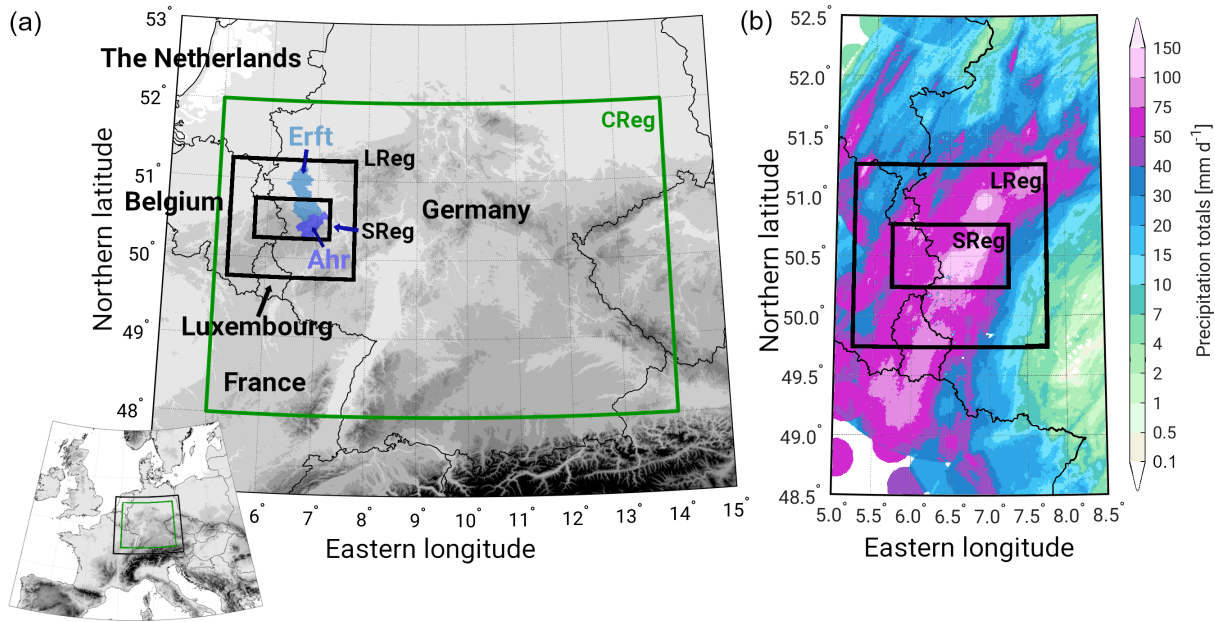


**Figure 1.** (a) Overview map of central and western Europe (bottom left) with a zoom-in on the region of interest, and (b) 24-hour precipitation totals of the 14 July 2021 based on RADOLAN (cf. [PART1](#)[PART 1](#)). Two regions (LReg, SReg; black rectangles) covering the main precipitation area and the affected river catchments of the Ahr (dark blue) and the Erft (light blue) are defined to derive specific event characteristics (e.g., spatial means). Analyses in a statistical and climatological context are performed over the greater central Germany region (CReg, green box). Topographic data (grey) were provided by NOAA National Geophysical Data Center (Amante and Eakins, 2008).

- (III) How would the [July specific extreme event of July 2021 precipitation event](#) unfold under different past and future climatic conditions and what implications [have these scenarios](#) [do these scenarios have](#) on flood events?
- (IV) How are precipitation characteristics (e.g., intensity, extent, [frequency](#)) projected to change [in general](#) under future climate conditions?

125 The structure of [PART2](#)[PART 2](#) is as follows: the data sets, models, and methods are described in Sect. 2. The classification into the historical context is presented in Sect. 3. Section 4 focuses on the possible role of climate change for the event and future projections. Finally, the discussion, summary, conclusions, and outlook are presented in Sect. 5.

## 2 Data and methods

130 In [PART2](#)[In PART 2](#), three rectangular [boxes](#) [geographical domains](#) are defined for both the event characterization and the statistical analysis. For a long-term climatological and statistical analysis, we define the CReg area (green rectangular in Fig. 1a) covering central Germany and parts of neighboring countries between 5° E and 14° E, and between 48° N and 52° N with about 285 000 km<sup>2</sup>. Although the [July 2021](#) event primarily affected western Germany, our intention is to identify comparable heavy

precipitation events across Germany in terms of spatio-temporal extent, precipitation totals, and antecedent conditions. CReg is characterized by similar topographic features such as low-mountain ranges resulting in similar orographic forcing during 135 precipitation formation or intensification. Furthermore, CReg is a region with hydroclimatic conditions comparable to the Ahr and Erft river basins such that analyses of both extreme rainfall and flood events can serve as a comprehensive spatio-temporal context for the 2021 flood event.

To characterize the July 2021 event more specifically, two additional smaller regions are defined based on the precipitation 140 observations and most affected areas of the Ahr and Erft river catchments: The larger event area (LReg, see Fig. 1) ranges between  $5.25^{\circ}$  E and  $7.75^{\circ}$  E, and from  $49.75^{\circ}$  N to  $51.25^{\circ}$  N covering an area of approx.  $30\,000\text{ km}^2$ . The smaller event area (SReg) ranges between  $5.75^{\circ}$  E and  $7.25^{\circ}$  E, and from  $50.25^{\circ}$  N to  $50.75^{\circ}$  N with a covered area of approx.  $6000\text{ km}^2$ .

The investigated period, in general, is determined by the length of the used data sets (see below). For the historical classification, all available data are used, the July 2021 event itself is characterized temporally using the 24 hours from 14 July 2021 05:50 UTC to 15 July 2021 05:50 UTC.

## 145 2.1 Observational data

### 2.1.1 Precipitation data

In line with ~~PART1~~<sup>PART 1</sup>, two different gridded precipitation data sets provided by Deutscher Wetterdienst (DWD) are used in this study: daily HYRAS data (*Hydrometeorologische Rasterdatensätze*; Rauthe et al., 2013), and hourly RADOLAN data (*Radar-Online-Aneichung*; Weigl and Winterrath, 2009; Winterrath et al., 2018). HYRAS includes daily precipitation totals at 150 a  $5 \times 5\text{ km}^2$  grid resolution covering Germany and its relevant river basin in neighboring countries for the period from 1951 to 2015 (update in preparation by DWD). HYRAS is based on station measurements interpolated to the regular grid considering local characteristics such as elevation or exposition. A sub-sample of HYRAS ~~are~~<sup>is</sup> the HYRAS-DE data, formerly known as REGNIE (*Regionalisierte Niederschlagshöhen*), covering only Germany but with a higher resolution of  $1\text{ km}^2$  and continuous updates on a daily basis. While HYRAS with its larger spatial extent was used for the bias correction of the high-resolution 155 regional climate simulations (see Sect. 2.2.1), HYRAS-DE is used to find comparable historical events in Germany due to the longer time period covered.

RADOLAN is a radar-based near-real-time precipitation data set covering Germany and parts of the neighboring countries with roughly  $1\text{ km}^2$  horizontal and hourly temporal resolution available since 2001. To account for uncertainties and typical radar artifacts, the radar-based precipitation rates are calibrated using hourly data ~~of~~<sup>from</sup> over 1000 ground-based observational 160 stations. RADOLAN is used to derive the precipitation totals of the July 2021 event due to its spatio-temporal availability.

### 2.1.2 River gauge data

In this study, we analyze river gauge data with the two objectives of, first, assessing the rarity of the 2021 flood event by comparing it to a large number of historical flood recordings from catchments in a similar hydroclimate, and second, assessing how the 2021 flood event might unfold under a further changing climate. For the first, we collected three data sets from the

165 Global Runoff Data Center (GRDC), the *Landesanstalt für Umwelt Baden-Württemberg* (LUBW), and peak flow estimates of historical floods at gauge Altenahr (Ahr). For the second, we fed rainfall from PGW scenarios into the hydrological model LARSIM to generate streamflow scenarios in a changing climate. For both objectives, we used observed and reconstructed streamflow data of the 2021 flood event for comparison. The data sets are explained in the following.

170 As described in detail in [PART1](#), we collected water level and streamflow data of ten river gauges for the 2021 flood event, covering the study area LReg (see Fig. 1) from the river Wupper in the east to the river Prüm in the west. These gauges cover a range of basin sizes from 31.9 km<sup>2</sup> at gauge Schöna (river Erft) to 816 km<sup>2</sup> at gauge Kordel (river Kyll). The gauge locations are shown in [PART1](#), Figure 1, water level and streamflow time series during the 2021 event are shown in [PART1 \(Fig. 5\)](#), Figure 5. Please note that a considerable portion of the streamflow values are reconstructions rather than observations, as many gauges were destroyed during the flood. Further information on the gauge data and gauge properties, such as basin size, historical extremes, and the discharge estimates of the 2021 flood event are also listed in [PART1](#) and historical extremes are listed in [PART1](#) (Table 1). Henceforth, we refer to these data as the 2021 gauge data (2021GD). All data were provided by the water administrations of Rhineland-Palatinate (LfU), the *Erftverband*, the *Erftverband*, and the *Wupperverband*.

175 To put the 2021 flood into a broader historical context, we utilized three further hydrological data sets. The first The GRDC data set is a collection of all streamflow data in the greater central Germany region (CReg, see Fig. 1) available from the Global Runoff Data Center (GRDC). To ensure comparability with the 2021GD, we restricted our sample to basin sizes up to 1000 km<sup>2</sup>. The 124 gauge time series available from GRDC fulfilling this criterion cover on average 69 years adding up to 9799 years of observations in total. From each time series of mean daily streamflow in m<sup>3</sup> s<sup>-1</sup>, we extracted the maximum value, i.e., the highest flood on record for each gauge. These maxima serve as an empirical upper bound for peak streamflow as a function of basin size. Henceforth, we refer to this data set as GRDC data.

180 The second LUBW data set was taken into account to classify the peak flows observed in 2021 in terms of statistical return periods. As a reference, we used peak discharge magnitudes for statistical return periods of 100, 200, 500, 1000, 5000, and 10 000 years (henceforth HQ<sub>100</sub>, HQ<sub>200</sub>, etc.) provided by the *Landesanstalt für Umwelt Baden-Württemberg* (LUBW) for all river gauges in the federal state of Baden-Württemberg. Ideally, such gauge data should have been used from the entire CReg region rather than from Baden-Württemberg only. However, as the CReg region extends over several federal states, and as the water administration in Germany is under the responsibility of the federal states, it is impossible to gather flood return times consistent flood return periods for all gauges in the CReg region based on the same approach of extreme value statistics due to the water administration in Germany being under the responsibility of the federal states with varying technical and statistical approaches. As Baden-Württemberg has a large spatial overlap with the CReg region, we considered this data set, comprising overall 355 gauges as a suitable basis to derive robust estimates of the relation between the magnitude of the 100-year flood and floods of higher return periods. We will refer to this data set as LUBW data in the text. Please note that while the GRDC data set is based on daily averaged data, the LUBW data are based on hourly data. Therefore, the For this reason, we derive daily averages of the 2021GD is used as daily averages for comparison with the former and as hourly data GRDC data and hourly values for comparison with the latter LUBW data. As mentioned in [PART1](#), we do not attempt

200 to assign a particular return period to the event as the related uncertainties are very large. Nevertheless, we think there is an added value in ~~providing a broader classification using both~~ the LUBW and GRDC data for a better classification of the July 2021 event in the historical context.

205 The third data set contains peak discharge values of major floods between 1804 and 2021 at gauge Altenahr (Ahr) – one of the basins most severely affected by the 2021 flood (Roggenkamp and Herget, 2022). The data are based on gauge recordings since 1946, and on reconstructions before. We use this data set to put the 2021 flood at the Ahr River into a larger historical perspective of local floods.

## 2.2 Model simulations

### 2.2.1 The regional climate model COSMO-CLM

210 Two ensemble data sets using the non-hydrostatic model of the Consortium for Small-scale Modeling (COSMO) in climate mode COSMO-CLM (CCLM; Sørland et al., 2021; Baldauf et al., 2011) were considered. One of them, the LAERTES-EU large regional ensemble (Ehmele et al., 2020) consists of CCLM simulations at a resolution of  $0.22^\circ$  ( $\approx 25$  km). The simulations were performed within the MiKlip project (Marotzke et al., 2016), which developed an operational decadal prediction system based on the Max Planck Institute of Meteorology coupled Earth System Model (MPI-ESM) with a regional downscaling component (Feldmann et al., 2019). Several ensemble generations of initialized decadal hindcast simulations with a consistent 215 model chain were combined into the LAERTES-EU ensemble, which consists of about 12 500 simulation years covering the present-day climate (the 20th century and the beginning of the 21st century). Regarding the limited intrinsic predictability of the atmosphere of about 12 to 15 days (e.g., Lorenz, 1982; Dalcher and Kalnay, 1987; Zhang et al., 2019), the individual members of LAERTES-EU can be considered independent as each member has an unaccounted spin-up of a few days to about 2 months. A positive precipitation bias of LAERTES-EU compared to observations was identified by Ehmele et al. (2020), 220 hence, Ehmele et al. (2022) applied a bias correction via monthly quantile mapping using E-OBS (Haylock et al., 2008) as a reference, which reduced the bias significantly. By applying the bias-corrected LAERTES-EU ensemble to hydrologic modeling of major Central European river basins, Ehmele et al. (2022) showed that LAERTES-EU enables statistically robust estimations of extreme events with very high return periods.

225 To assess the effect of climate change on extreme precipitation intensities and their return ~~values-levels~~ over complex topography, very high-resolution climate simulations are needed (Feldmann et al., 2013; Prein et al., 2015). For this purpose, an ensemble of regional climate simulations with CCLM at convection-permitting (CPM) resolution of 2.8 km was produced and applied in the context of the KLIWA (*Klimaveränderung und Wasserwirtschaft*) project (Schädler et al., 2018; Hackenbruch et al., 2016) at KIT (hereafter referred to as KIT-KLIWA). The KIT-KLIWA ensemble consists of transient simulations covering the time period from 1971 to 2100. Four general circulation models (GCMs) from the Coupled Model Intercomparison 230 Project Phase 5 (CMIP5) (Taylor et al., 2012) using the Representative Concentration Pathway emission scenario 8.5 (Meinshausen et al., 2011, RCP8.5;) provided the boundary conditions for a three-step downscaling with CCLM, first to 50 km over Europe, second to 7 km over Germany, and finally to 2.8 km over Southern Germany south of  $52^\circ$  N. Subsequently, a bias

correction via monthly quantile mapping (Berg et al., 2012) was applied to the daily precipitation totals using the HYRAS data as a reference. An overview of the driving GCMs and realizations used for KIT-KLIWA can be found in Table S1 in 235 the supplementary material. The KIT-KLIWA simulations are analyzed regarding the extreme precipitation in a present-day reference period (1971 to 2000) and their changes under a global warming level (GWL) of +2 K and +3 K (hereafter GWL2 and GWL3) with respect to pre-industrial (1881 to 1910) climate conditions. The method was adopted from Teichmann et al. 240 (2018), who defined the GWL as a 30-year period centered around the year in which a GCM reaches the GWL for the first time. Consequently, this time period varies between the different GCMs used, but as a result, they represent similar climatic conditions. The GWL time periods in the respective GCMs can be found in Table S1. ~~The GWL of the present-day reference period based on global observations is +0.46 K (Teichmann et al., 2018).~~ Note that the GWL refers to a global average and that regional warming levels might deviate from this.

## 2.2.2 Pseudo-global-warming experiments with WRF

To assess how the ~~flood event could 2021 event would~~ potentially unfold in the context of climate change, a storyline approach 245 is applied (Shepherd, 2016). This approach complements the above-described probabilistic concept based on ensembles of (regional) climate model simulations to cope with the uncertainty in physical aspects of climate change. ~~Additionally, this approach allows us to estimate the precipitation scaling for this specific event when increasing/decreasing the temperature and humidity (based on the CC-scaling) in the initial and forcing data. However, the precipitation scaling does not necessarily have to follow the CC-scaling, as physical process (e.g., latent heat release feedback; Lenderink et al., 2017) can modify the moisture conversion, thus leading to super CC-scaling behavior.~~ With that, a series of PGW experiments with the WRF model 250 (version 4.3; Skamarock et al., 2019) were performed. A control simulation at a CPM horizontal grid spacing of 0.0275° (≈ 2.8 km) driven by the fifth generation European Centre for Medium-Range Weather Forecasts (ECMWF) atmospheric re-analysis data (ERA5; Hersbach et al., 2020) was conducted to test the capability of the WRF model to simulate the precipitation event appropriately. All WRF simulations were initialized on 14 July 2021, 00:00 UTC and ran for 30 hours until 15 July 2021, 255 06:00 UTC with boundary conditions being updated hourly. To ensure that the simulated ~~flood triggering~~ ~~flood-triggering~~ cyclone remains over the affected area, spectral nudging (von Storch et al., 2000) was applied to the large-scale wind fields above the planetary boundary layer. To account for the physical processes that are not explicitly resolved by the model, we used the following parameterization schemes: the rapid radiative transfer model RRTMG for shortwave and longwave radiations (Iacono et al., 2008), the Thompson microphysics scheme (Thompson et al., 2008), Zhang et al. (2011), the Mellor-Yamada- 260 Janjic (MYJ) planetary boundary layer scheme (Janjić, 1994), the Noah land surface model (Chen et al., 1997), and the MYJ surface layer scheme (Janjić, 1994). For the PGW experiments, the control simulation was repeated with changes in the ERA5 initial and boundary conditions. In total, we performed ten additional PGW experiments, with the temperatures of the initial and boundary data from ERA5 being either reduced to -2 K or increased to +3 K at an interval of 0.5 K. ~~A~~ ~~The control run (± 0 K) uses the present-day conditions, which represent a global warming level of already + 1.09 K (GWL1) according to IPCC (2022).~~ Thus, a reduction of 1 K would represent temperatures as in the pre-industrial period (GWL0), while an increase 265 of 2 K corresponds to GWL3. The relative humidity was kept constant by reducing or increasing the specific humidity of the

initial and boundary data based on the Clausius-Clapeyron (CC) relationship, which describes that for every 1 degree increase in temperature, there is an increase in humidity of 7 %.

### 2.2.3 Hydrological simulations with LARSIM

270 The results of the PGW simulations described in the previous section are used for additional hydrological modeling and analyses. Therefore, the operational flood forecasting model based on the hydrological Large Area Runoff Simulation Model (LARSIM) (Ludwig and Bremicker, 2006) for RP is used, which is operated by the water administration of RP. LARSIM is a semi-distributed, physics-based conceptual water balance model that captures all relevant processes related to the terrestrial water cycle and operates in hourly resolution. In Germany, it is in widespread use for operational flood forecasting and water 275 balance modeling. For the PGW-based studies, the LARSIM model is used for the Ahr river upstream of gauge Altenahr (hereafter LARSIM-Ahr). The LARSIM-Ahr model consists of 561 subbasins with an average area of 1.6 km<sup>2</sup> per subbasin.

Three different simulations are performed with LARSIM-Ahr. The first run was forced with a spatially distributed rainfall product as presented by Bardossy et al. (2022). It is based on a comprehensive post-event collected set of rain gauge recordings from both public and private weather stations, and rainfall estimates based on the signal attenuation in mobile phone networks.

280 A comparison with radar-based rainfall estimates and estimates from public rain gauges only (Regenauer et al., 2022) demonstrated that this product allowed the most accurate simulation of the reconstructed flood peak at Altenahr. Hence, this reference was used as a basis for the hydrological PGW experiments. For the other two LARSIM-Ahr simulations, the PGW relations for -1 K (pre-industrial) and +2 K (GWL3) are used.

## 2.3 Methods

### 285 2.3.1 Return ~~values~~ levels and periods

For both observations and model data, the return period (RP)  $T_{RP}(x)$  of a precipitation event  $x$  or, vice versa, the return ~~value~~ level for a given return period  $x_{RP}(T)$  is derived using extreme value statistics. In line with ~~PART1~~ PART 1, we used the three-parameter generalized Pareto distribution (GPD) and applied it to the KIT-KLIWA climate model ensemble (see Sect. 2.2.1) using the peaks-over-threshold (POT) approach (e.g., Wilks, 2006). The scale and shape parameters of the 290 GPD were estimated using maximum likelihood estimation (MLE), while the 95 % percentile of the considered data series was used as the location parameter. After estimating the parameters, the statistical relation between the cumulative density function of the GPD  $F_{GPD}$  and the corresponding return period  $T$  can be expressed as  $T = [\lambda \cdot (1 - F_{GPD})]^{-1}$  (e.g., Madsen et al., 1997; Brabson and Palutikof, 2000), where  $\lambda$  is the crossing rate (average number of events per year).

Adjusting such a statistical distribution function to a data series ~~allows for extrapolating short data sets to higher return periods and also~~ reduces the statistical uncertainty compared to an empirical return period estimation such as the block maximum method (e.g. Bezak et al., 2014). Furthermore, ~~it allows for extrapolating the analyses to higher return periods beyond the length of the given time series which is useful for comparatively short data sets like observations (e.g., Grieser et al., 2007). However, the uncertainty of this extrapolation rapidly increases in this uncovered range of values. Following the study of~~

Früh et al. (2010), who found reasonable results of extreme value statistics (e.g. Grieser et al., 2007; Bezak et al., 2014).  
300 Following Früh et al. (2010), reasonable results can be obtained for return periods of up to one-third of the length of the time series, we focus on the 10-year return value in the case of KIT-KLIWA.

In contrast to adjusting a statistical distribution, the empirical approach was applied to the LAERTES-EU data to determine return values levels and periods up to 1000 years, which is adequate due to the large data amount of about 12 500 years. In this case, the return period estimation simplifies to  $T = L \cdot N^{-1}$ , where  $L$  is the length of the data series and  $N$  is the number of  
305 occurrences (Gumbel, 1941).

### 2.3.2 Precipitation indices

In addition to the antecedent precipitation index (API) used in PART1, two other measures are PART1, the empirical heavy precipitation event criterion  $HPE_{crit}$  is applied to the HYRAS-DE data for the classification of precipitation events: the first one is the empirical heavy precipitation event criterion  $HPE_{crit}$ , which combines thresholds for magnitude and extension  
310 based on daily precipitation totals. A special feature of the July 2021 event was the rather wide area with high precipitation totals exceeding the 50-year return level (cf. PART1, Fig. according to the KOSTRA data (see supplemental material and cf. PART1, Figure S3), which, in combination with the hydrological and hydro-morphological conditions on-site, resulted in this exceptional event. Therefore, an For  $HPE_{crit}$ , first, the 50-year return level of a KOSTRA grid cell ( $8 \times 8 \text{ km}^2$ ) is assigned to all HYRAS-DE grid cells ( $1 \times 1 \text{ km}^2$ ) that are geographically located in the same KOSTRA grid cell. Second, all contiguous  
315 HYRAS-DE grid cells exceeding the threshold are counted (area  $A$ ). An event fulfilling  $HPE_{crit}$  is then defined when daily rainfall totals exceed the 50-year return level according to KOSTRA (cf. PART1, supplementary material) on a contiguous area  $A$  of at least  $1000 \text{ km}^2$ , representing roughly medium-size river catchments like the Ahr and the Erft. Thus, comparable precipitation events in terms of magnitude and the affected area can be identified and characterized.

The second measure used is the Precipitation Severity Index (PSI; Caldas-Alvarez et al., 2022b). It identifies extreme  
320 precipitation events based on three characteristics: grid point intensity, the affected area, and persistence. First, gridded daily precipitation totals from HYRAS-DE were divided by the climatological 80 % percentile of the corresponding grid point. For grid points exceeding a ratio of one, these ratios were spatially aggregated and normalized by the affected area. Finally, a temporal summation was applied to grid points exceeding a ratio of one for up to two days prior to the considered event day. The PSI has been successfully implemented in a recent study about heavy precipitation  
325 (Piper et al., 2016; Caldas-Alvarez et al., 2022b). Due to the temporal summation, the PSI tends to shift the day of maximum severity by one day compared to  $HPE_{crit}$ . Furthermore, PSI detects much more events due to the less restrictive thresholds used.

## 3 The July 2021 event in the historical context

As demonstrated in PART1PART1, the disastrous nature of the July 2021 event originated from interactions of atmospheric,  
330 hydrological, and hydro-morphological processes and mechanisms that have interacted “optimally” at different spatial and

temporal scales. In this section, we put these aspects of the event in a historical and statistical context to evaluate its rarity and to elaborate on probabilities of occurrence.

### 3.1 Meteorological perspective

For the classification of the July 2021 precipitation event in the historical context, we used (i) different thresholds and indices 335 to identify similar historical events from observational data sets, and (ii) the 12 500 years of the LAERTES-EU data to derive more comprehensive precipitation statistics under present-day climate conditions.

#### 3.1.1 Event-based analyses

Applying the HPE<sub>crit</sub> (Sect. 2.3.2) to the HYRAS-DE data set, in total 26 heavy precipitation events between 1951 and 2021 in Germany turned out to fulfill the criterion (see Table S2 in the supplementary material). The rainfall distribution distributions 340 of the eight most intense events are illustrated in Fig. 2, and the events ranked 9th to 20th–26th are displayed in Fig. S1 (see supplementary material). Please note that the actual total event area and precipitation might not be captured by HYRAS-DE in total when the event extended outside Germany. Such cases can not be captured by the presented analysis.

~~It is striking that almost all events took place during the warm season between May and September and that 11 of these 26 events occurred in the last 20. Among the list of HPE<sub>crit</sub> events, there are a few prominent ones that had a severe impact. 345 The precipitation event that led to the great Elbe flood in August years with three events in 2002 and three in 2021 alone (Table 2002 (ranked 3rd; e.g., Ulbrich et al., 2003), the Elbe and Danube floods from July S2). For the nine top-ranked events, the affected area (within Germany) covers between 6500–1954 (e.g., Schröter et al., 2015) with the related precipitation events ranked 9th and 21–23rd, the flood events in the Alpine region and along the river Rhine in May 000–1999 (e.g., Frei et al., 2000), which is ranked 15th, the Berlin event in June km<sup>2</sup>, while the spatial coverage of the lower-ranked events is below 4000–2017 350 (ranked 4th; e.g., Caldas-Alvarez et al., 2022a), or a precipitation event leading to flooding in the Oder river basin in August 1978 (ranked 1st; Marx, 1980).~~

~~The July 2021 event is ranked 5th (Fig. 2e) with approx. 8000 km<sup>2</sup>. Furthermore, the majority of events (20 out of 26; 77 above the 50-year return level. Regarding the spatial mean precipitation averaged over the HPE<sub>crit</sub> area A (100.2 %) affected the eastern and southeastern parts of Germany (Figs. mm) and the maximum grid point precipitation (154.3 2 and S1). This 355 weather pattern can be related to the typical Vb cyclone pathway (van Bebber, 1891) where cyclones move from the Gulf of Genoa in the western Mediterranean along the eastern foothills of the Alps towards central and eastern Europe. Mudelsee et al. (2004) and Messmer et al. (2015), for example, emphasized the role of the cyclone pathway Vb and the associated moisture transport on central European river floods during summer, especially in the eastern river basins of Elbe and Oder. The areas with high precipitation totals are usually located on the northern or western flank of these low-pressure 360 areas mm), the July 2021 is in the upper third of the events. Please note that the actual total event area and precipitation might not be fully captured by HYRAS-DE when the event is extended outside Germany. Hence, the position of the driving low-pressure system is crucial for the precipitation event reaching into the study area (namely Germany). This is the case for precipitation~~

events close to the border such as the 8 August 1978 (ranked 1st) or the 12 August 2002 (ranked 3rd). Especially in the latter, significant precipitation totals were registered outside Germany (namely in the Czech Republic; e.g., Ulbrich et al., 2003).-

365 The most intense precipitation events in Germany ranked 1st (a) to 8th (h) according to the  $HPE_{crit}$  criterion based on daily (05:50 UTC to 05:50 UTC) HYRAS-DE data from 1951 to 2021. The July 2021 event is ranked 5th (e). See also Table S2 for further statistics of the events.

The top-ranked event according to  $HPE_{crit}$  is the 8 August 1978, when heavy precipitation of more than 50 mm in 24 hours was registered over almost entire eastern Germany ( $\approx 21\,000 \text{ km}^2$ ; Fig. 2a) leading to a flood event in the Oder river basin 370 (Marx, 1980). The second-ranked event is the 17, but also in case of the July 2002 with an affected area of roughly  $13\,000 \text{ km}^2$  placed over northern Germany. Although highly ranked, no impact information could be found for this particular event which is probably related to the rather flat terrain and thus non-accumulating runoff opportunities in that region. The precipitation event that led to the great Elbe flood in August 2002 (e.g., Ulbrich et al., 2003) ranks 3rd with an affected area of approximately 2021 375 (e.g., Schäfer et al., 2021; Junghänel et al., 2021; Dewals et al., 2021; MeteoLux, 2021).

It is striking that almost all events took place during the warm season between May and September and that 11 of these 26 events occurred in the last  $20\,000 \text{ km}^2$ . This event is also characterized by the highest spatial mean and grid point precipitation. The Berlin event in June 2017 (Caldas-Alvarez et al., 2022a) ranks 4th (approx.  $10\,000 \text{ km}^2$ ). The July years with three events 380 in 2002 and three in 2021 event is ranked 5th (approx.  $8\,000 \text{ km}^2$ ) in this list (Fig. 2e). Other prominent events are the Elbe and Danube floods from July 1954 (Schröter et al., 2015, e.g.) with the related precipitation events ranked 9th and 23rd (approx. S2). For the nine top-ranked events, the affected area (within Germany) covers between  $6500$  and  $21 \text{ km}^2$  and  $1000\,000 \text{ km}^2$ ) and the flood events in the Alpine region and along the river Rhine in May 1999 (e.g., Frei et al., 2000), which is ranked 15th (approx.  $1700$ , while the spatial coverage of the lower-ranked events is below  $4000 \text{ km}^2$ ).

Looking at the spatial distribution of the most intense events reveals two main types of precipitation fields (Figs. 2 and S1). Furthermore, 385 the majority of events (20 out of 26; 77%) affected regions in northern, eastern, or southern Germany with some regions being affected multiple times (Figs. 2 and S1a–h). The second type shows a rather small band of very high precipitation intensities (above 75). Hence, the July  $\text{mm d}^{-1}$  also embedded in different-sized fields of low to moderate intensities. Examples for this type are shown in Fig. 2e, f, and h, and Fig. S1i–l. The 390 July 2021 event (Fig. S1e) shows characteristics of the latter. Note that both types may contain both synoptic-scale precipitation and embedded convection, was unique for that particular western part of Germany.

For the same list of events, the PSI (Sect. 2.3.2) and API (supplementary material) were additionally calculated. Normalized Antecedent Precipitation Index (NAPI; see supplementary material) was additionally calculated over the  $HPE_{crit}$  area A in order to better capture the preconditions and persistence of the events and their possible role on the impacts. 395 Furthermore, the events were ranked according to their PSI values to compare the results to the  $HPE_{crit}$  analysis. While there are only minor changes in the order of the top events, the ranking is more diverse for the less-extreme events (see Table S2).

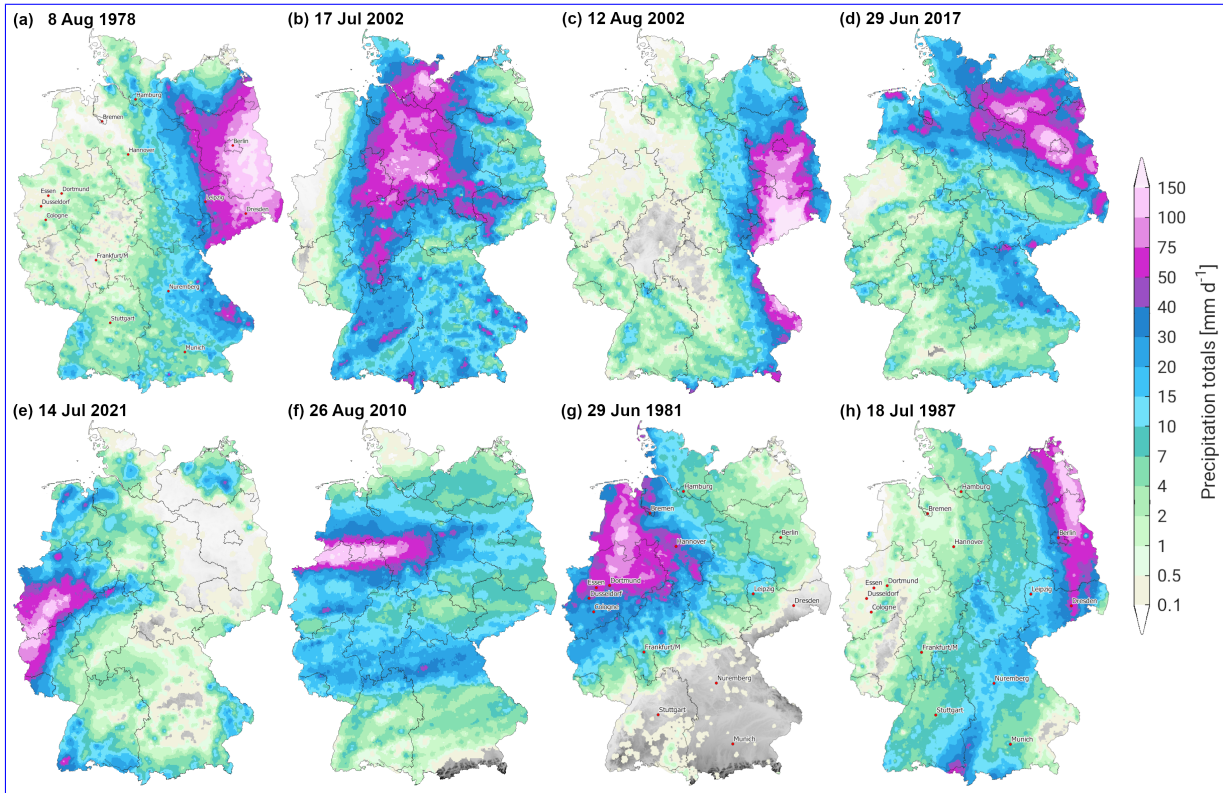


**Figure 2.** The most intense precipitation events in Germany ranked 1st (a) to 8th (h) according to the  $HPE_{crit}$  criterion based on daily (05:50 UTC to 05:50 UTC) HYRAS-DE data from 1951 to 2021. The July 2021 event is ranked 5th (e). See also Table S2 for further statistics of the events.

The July 2021 event even ranks only 23rd in the PSI analysis, which is mainly a result of the temporal summation (absence of persistence) applied in the PSI calculation.

Figure ?? shows the maximum intensities 3 shows the NAPI (bubble size) in relation to the soil moisture prior to the initiation 400 spatial mean and the maximum grid point precipitation also calculated over  $A$ . The majority of the events expressed by the Normalized Antecedent Precipitation Index (NAPI; see supplementary material Seet, about 65  $A$ ). NAPI was calculated on and averaged over the same grid points as PSI. There is a cluster of events at dry to %) have a NAPI between 0 and 2 meaning that the events occurred after normal or slightly wet preconditions (NAPI between 0.0 and 2.0) and medium severity (PSI between 0.5 and 1.5). The July 2021 event (PSI rank 23) classifies into this cluster in the less severe but slightly too wet 405 corner. A second cluster appears for wetter preconditions (NAPI around 3.0) and medium severity. Note that the isolated event of too wet periods compared to the climatology. Furthermore, most events show a linear relation between spatial mean and maximum intensity indicating a more homogeneous distribution of precipitation intensities within  $A$ . Some of the most extreme events according to  $HPE_{crit}$  (namely rank 2 to 5, 7, and 9 including the July 1954 (PSI rank 3,  $HPE_{crit}$  rank 23) results

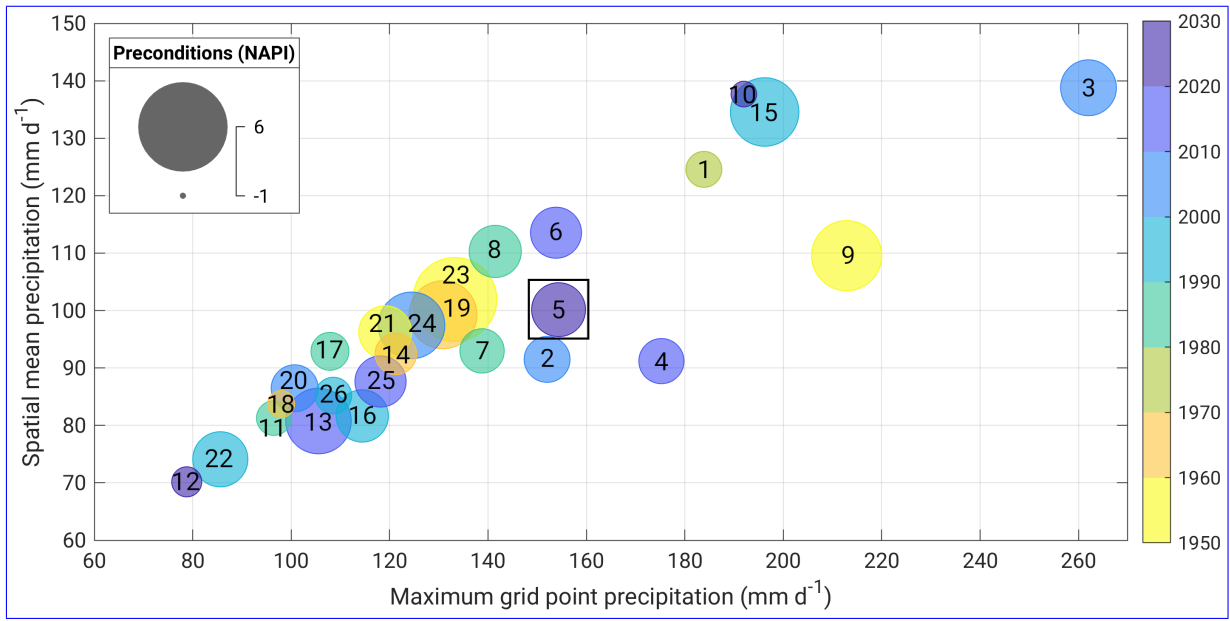


**Figure 3.** Bubble plot of the most extreme precipitation events in Germany according to the  $HPE_{crit}$  based on daily HYRAS-DE data (1951 to 2021). The ~~severity (PSI) maximum 24-hour grid point intensity within the  $HPE_{crit}$  area  $A$~~  is given on the ~~y-axis~~<sup>x-axis</sup>; the ~~x-axis~~<sup>y-axis</sup> represents the ~~spatially averaged 24-hour precipitation over  $A$~~ . The size of the bubbles (small inset legend at the top left) represents the ~~maximum daily grid point precipitation (small inset legend at the bottom right)~~, while the color indicates the decade of occurrence. The numbers give the ranking according to the ~~PSI analysis  $HPE_{crit}$~~  (see Table S2). The July 2021 event (ranked ~~23rd~~<sup>5th</sup>) is marked with a rectangle.

410 from a persistent precipitation regime that brought already heavy precipitation on ~~8~~<sup>2021</sup> event) show an emphasis towards higher locally enhanced precipitation maximums and, therefore, are located more to the right in Fig. July 1954 ( $HPE_{crit}$  rank 9) leading to very high NAPI values ~~3~~<sup>3</sup>. This intensification can often be related to embedded convection initiated by orography (e.g., Fuhrer and Schär, 2005; Cannon et al., 2012) or frontal systems (e.g., Trier et al., 1991; Weckwerth and Parsons, 2006).

415 The aforementioned results of the precipitation fields and PSI analyses pointed out a higher level of diversity among the top events in Germany regarding intensity, affected area, and duration. To investigate the relation of the former two in more detail, the same set of top events is mean and maximum intensity, and affected area. The relation between intensity and extent is now analyzed determining the spatial mean daily precipitation totals on different area dimensions based on HYRAS-DE (Fig. 4). Therefore, we continuously increased the precipitation threshold from 0 mm to event maximum and determined the area of contiguous grid cells that exceeded this threshold. The majority of events accumulate in a band ranging from 95 to 130  $mm\ d^{-1}$  on an area of  $100\ km^2$ , and 75 to  $110\ mm\ d^{-1}$  on  $1000\ km^2$  to a range of 40 to  $80\ mm\ d^{-1}$  on  $10\ 000\ km^2$  (Fig. 4, gray-shaded area). The top eight events are mostly located above this band (Fig. 4, colored lines). The top-ranked event (according to the  $HPE_{crit}$ ) of 8 August 1978, for example, is placed well above this band up to area dimensions of  $50\ 000\ km^2$  (Fig. 4, black

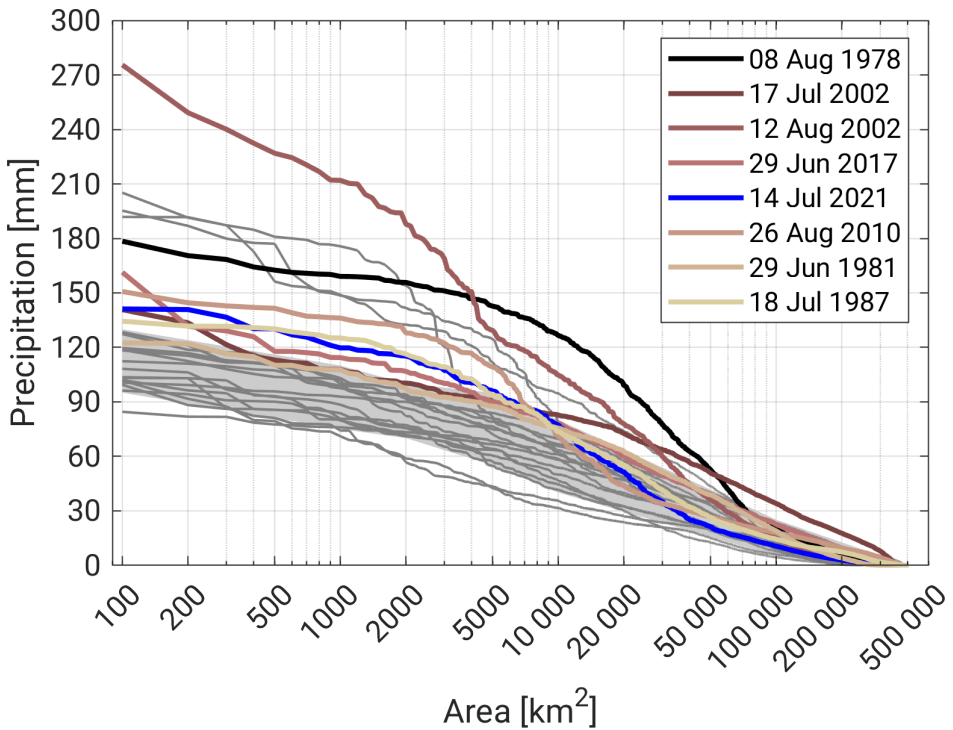


**Figure 4.** Relationship between precipitation totals and affected area (contiguous grid cells) for the 26 strongest precipitation events in Germany based on HYRAS-DE (1951 to 2021) applying the  $HPE_{crit}$  criterion (see Table S2). The colored lines represent the top eight events (same as in Fig. 2) with the blue line indicating the July 2021 event. The shaded area marks the range in which more than 50 % of the events are located.

line). For smaller areas below  $4000 \text{ km}^2$ , the event of 12 August 2002 ( $HPE_{crit}$  rank 3) is outstanding. The July 2021 event (Fig. 4, blue line) is also located above the majority band for areas up to  $10000 \text{ km}^2$  and within this band for extensions above. For areas above approx.  $30000 \text{ km}^2$ , the July 2021 event is even placed at the lower boundary of the majority band. Figure 4 underpins the previously shown results in the sense that the July 2021 event was special but not exceptional on small to medium spatial scales regarding the precipitation intensities compared to other historical events.

### 3.1.2 Statistical analyses

In order to derive more comprehensive statistics of precipitation events, the 12 500 years of bias-corrected LAERTES-EU data were used considering the total area CReg. In doing so, the spatial representativeness of the derived statistics is increased and the influence of events occurring randomly at a specific local position is limited. The observed values of the July 2021 event were taken from RADOLAN, which in this context was interpolated to the  $0.22^\circ$  grid of LAERTES-EU for better comparison.

The relation between precipitation intensity and the affected area for 24-hour precipitation totals and different return [intervals](#) [periods](#) within LAERTES-EU is shown in Fig. 5. Similar to Fig. 4, we continuously increased the precipitation threshold

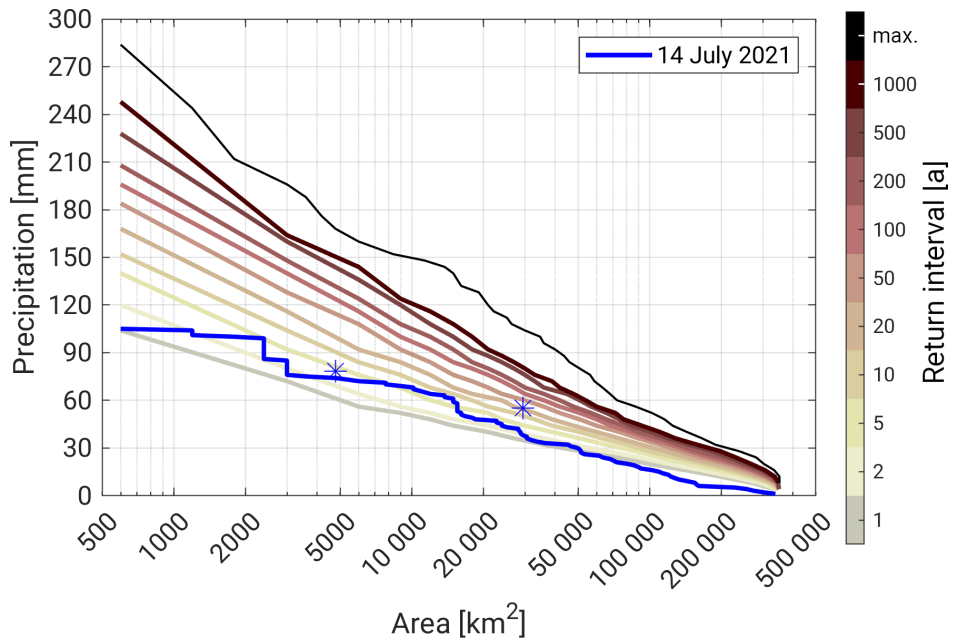


**Figure 5.** Empirical return *intervals-periods* (colored curves) estimated from the bias-corrected LAERTES-EU data set for precipitation clusters (affected area of contiguous grid points, x-axis) above certain precipitation thresholds (y-axis) for 24-hour totals. The uppermost solid black line represents the maximum values within LAERTES-EU equivalent to a return *interval-period* of one in 12,500 years. The blue curve represents the July 2021 event (based on RADOLAN interpolated to the  $0.22^\circ$  grid); the two blue marks indicate the spatial means for LReg and SReg.

and determined the area of contiguous grid cells exceeding this threshold. In a second step, the number of occurrences of each area–intensity–combination within the 12 500 years of LAERTES-EU is counted which then can be converted to return *intervals-periods*. The maximum return *interval-period* of roughly 10 years was reached for a contiguous area of approx. 15 000  $\text{km}^2$  with all grid points having 60 mm or more (Fig. 5, blue line). Most of the other size ranges are below the 2-year return level. Using the fixed-sized SReg and LReg areas (Fig. 5, blue marks), the spatial mean precipitation according to RADOLAN during the July 2021 event was 78.4 mm in 24 hours for SReg corresponding to a return *interval-period* of 5 years according to LAERTES-EU. For the larger LReg, the observed spatial mean of 55.2–55.4 mm corresponds to a return *interval-period* of 20 years. Considering only LAERTES-EU data for LReg or SReg, the return *intervals-periods* are between 100 and 200 years (not shown) which confirms the result of the previous section that most of the events took place in eastern and southern Germany (Sect. 3.1.1). ~~However, comparing the results to the findings in PART1 or Kreienkamp et al. (2021), who both estimated return periods for the event of several hundred to 1000 years based on observations, clearly highlights the uncertainty of a return period estimation solely based on such (short-termed) data sets or for specific areas. Although being exceptional for that particular region, comparable precipitation events occur more frequently in a statistical sense anywhere within CReg.~~

The results of the spatial analysis are in line with those of PART1–PART 1 and the findings of the previous section that the ~~extent of the July 2021 precipitation field~~ ~~location of the extended precipitation field of the July 2021 event~~ was special. Furthermore, PART1–PART 1 illustrated that some members of the DWD weather forecast ensemble ICON-D2-EPS predicted even higher precipitation totals in the LReg region (cf. PART1–PART 1, Fig. 4). The maximum predicted spatial mean precipitation amount for LReg was 78.4 mm in 24 hours, which has an equivalent return ~~interval period~~ even in LAERTES-EU of 500 to 1000 years when considering the total CReg area (3000 years when considering LReg data only) indicating the hazardous potential of the atmospheric conditions.

In order to also classify and contextualize the above-mentioned results in the context of the 2021 event, the 26 top-ranked historical events analyzed in the previous section were also put into the statistical LAERTES-EU context deriving the maximum precipitation return ~~interval period~~ and the affected area by this return level (see Table S2, last two columns). The top events show diverse characteristics with return ~~intervals periods~~ between less than 1 year and more than 1000 years for areas between 500 and 80 000 km<sup>2</sup>. Compared to the July 2021 event, there were historical events, for which a lower maximum return ~~interval period~~ was reached at larger affected areas and vice versa. However, only two other events (8 August 1978, HPE<sub>crit</sub> ranked 1st; and 17 July 2002, HPE<sub>crit</sub> ranked 8th) reached the same order of return ~~interval period~~ (50 or more years) over a comparable order of area size (10 000 to 20 000 km<sup>2</sup>), emphasizing that this combination of occurrence probability and extent was exceptional during the July 2021 event.

### 3.2 Hydrological perspective

In this section, different discharge gauging data sets are used to first classify the July 2021 flood event in a statistical context in the greater CReg region. In ~~a~~<sup>the</sup> second step, historical records for the mainly affected Ahr Valley are used to specify the flood in this particular region.

#### 3.2.1 Comparison to GRDC data

In Figure 6, the ~~peak streamflow values (mean daily value) daily mean peak streamflows~~ of the 2021GD (in red) and the GRDC data (in blue) are shown as a function of basin size (up to 1000 km<sup>2</sup>). For ~~both data sets, a strong and approximately the latter, the maximum daily mean value in the data set for each gauge is used. Both data sets show a~~ linear dependency between peak streamflow and basin size ~~is visible~~. The 2021GD ~~values~~ clearly appear at the upper envelope of the GRDC data ~~only exceeded by five peak values from the GRDC data set. All peak values come from gauges located in mountainous regions with steep terrain and above-average rainfall, favoring unusually high flood peaks. Two of these peak values were recorded in the Ore mountains at gauge Dohna (Müglitz) and gauge Pockau (Flöha) during the disastrous flood in August 2002 (e.g., Ulbrich et al., 2003)~~. For an objective assessment of the placement of the 2021GD data in the GRDC data, we first calculated for each gauge the specific peak streamflow by dividing the peak streamflow by the upstream catchment size and then ordered the gauges in descending order. Out of the overall 152 values, the 2021GD data received an average rank of 22.8, which is ~~among the top rainfall events shown in Fig. clearly above the mean rank of 152/2 = 76~~. At several gauges, even the daily mean streamflow (Table 2 (e)). The other three peak values were recorded at gauges in the Black Forest in southwestern

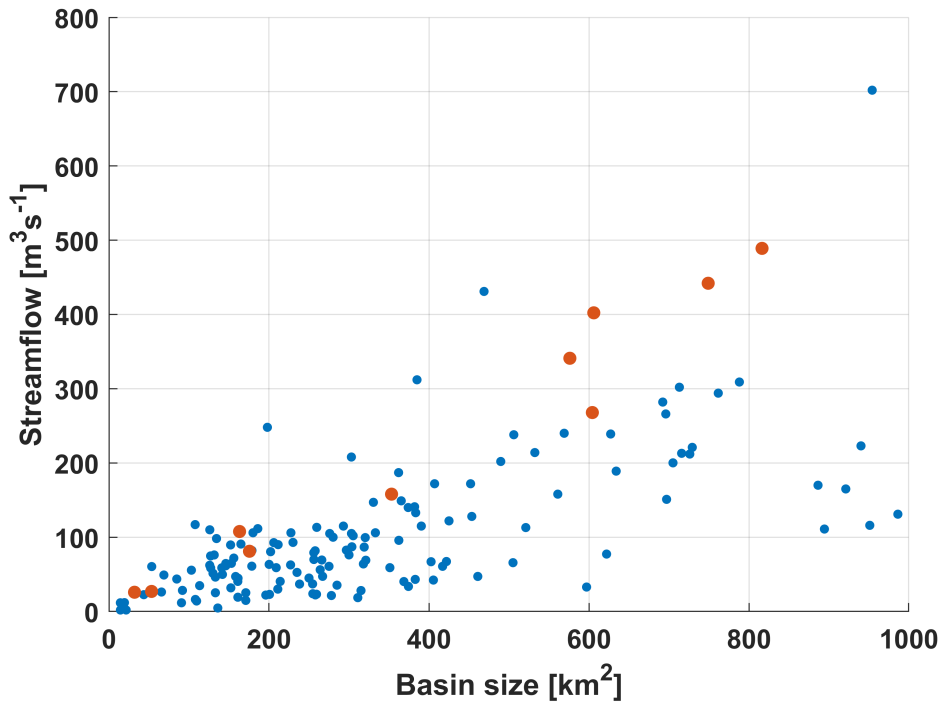


**Figure 6.** Relation between basin size and daily mean streamflow for the maximum recorded mean daily values from 124 gauges in the CReg region (GRDC data set; blue dots) and the estimated maximum values of the 2021 flood event at ten gauges in the LReg area (2021GD; red dots). For GRDC, the maximum daily mean streamflow for each gauge in the data set is used (see also Table 1). The location of the latter 2021GD stations is shown in PART 1, Figure 1, and additional information is given in PART 1, Table 1.

480 Germany for floods in 1919 at gauge Schwaibach (Kinzig), 1947 at gauge Bad Rothenfels (Murg), and 1991 at gauge Gutach (Elz) 1 exceeded the statistical 100-year return level ( $HQ_{100}$ ). Overall, this underlines the exceptional nature of the 2021 flood event, especially when bearing in mind that the total number of observations in the GRDC data sets covers almost 10 000 years of observations.

### 3.2.2 Comparison to LUBW data

485 In this section, we put the 2021GD set into the perspective of floods with given return periods. To do so, we first calculated for each 2021GD gauge the ratio between the 2021 peak flow and the gauge-specific  $HQ_{100}$  value (cf. also PART 1, Table 1). We used the  $HQ_{100}$  value as a reference as it is (i) a widely used design value (e.g., LUBW, 2005), and (ii) as it should be a relatively robust statistical measure given the on average 51 years of observation at the gauges. The peak factors are shown in Table 1. Please note that we use the estimate of 900 to 1000  $m^3 s^{-1}$  provided by the water administration of RP (cf. 490 PART 1, Sect. 3.2) rather than the estimate of 1000 to 1200  $m^3 s^{-1}$  based on hydraulic considerations by Roggenkamp and Herget (2022) for the peak discharge and peak factor calculation at gauge Altenahr (Ahr).

**Table 1.** Gauges of the 2021GD data set in the LReg area (adopted from PART1, Table 1).  $\overline{Q}_{100}$ :  $\overline{Q}_{24h,2021}$  indicates a flood with a statistical 100-year return period, the daily mean streamflow and  $Q_{max,2021}$  is the peak discharge of the July 2021 flood event (values are estimates),  $\overline{Q}_{100}$  indicates a flood with a statistical 100-year return period. The peak factor PF is defined as  $Q_{max,2021}$  divided by  $Q_{100}$ . Additionally, the upstream catchment size  $A_{upstream}$  is given.

Gauge /river name(river name)	$\overline{Q}_{100}$ $\overline{Q}_{24h,2021}$ ( $m^3 s^{-1}$ )	$Q_{max,2021}$	PF ( $m^3 s^{-1}$ )	$\overline{Q}_{100}$ ( $m^3 s^{-1}$ )	PF	$A_{upstream}$ ( $km^2$ )
Müschen /Ahr(Ahr)	152.0 158		≈ 500	152.0	≈ 3.3	353
Altenahr /Ahr(Ahr)	241.0 442		≈ 1000	241.0	≈ 4.0	749
Jünkerath /Kyll(Kyll)	118.0 81		≈ 200	118.0	≈ 1.7	175
Kordel /Kyll(Kyll)	248.0 489		≈ 600	248.0	≈ 2.5	816
Prüm 2 /Prüm	51.6 27		≈ 120	51.6	≈ 2.3	53
Prümzurlay /Prüm	278.0 341		≈ 600	278.0	≈ 2.0	576
Schönau /Erft(Erft)	19.0 26		≈ 100	19.0	≈ 5.2	31
Bliesheim /Erft(Erft)	71.0 268		≈ 500	71.0	≈ 7.3	604
Hückeswagen /Wupper(Wupper)	73.0 108		≈ 200	73.0	≈ 2.9	163
Opladen /Wupper(Wupper)	250.0 402		≈ 530	250.0	≈ 2.1	606

**Table 2.** Statistical peak factors PF for the LUBW data set. The statistical peak factor is defined as  $Q_{HX}$  ( $X = 200, 500, 1000, 5000, 10\,000$ ) divided by  $Q_{100}$ , separately for each gauge in the data set.  $PF_{mean}$  is the mean peak factor of all 355 gauges, and  $PF_{max}$  is the largest factor.

	PF <sub>mean</sub>	PF <sub>max</sub>
$Q_{200}$	1.13	1.22
$Q_{500}$	1.32	1.53
$Q_{1000}$	1.47	1.83
$Q_{5000}$	1.63	2.23
$Q_{10\,000}$	1.86	2.84

At all 2021GD gauges, the 2021 flood clearly exceeded the  $Q_{100}$ , indicated by all peak factors exceeding the value of one, ranging from 1.7 at gauge Jünkerath (river Kyll) to 7.3 at gauge Bliesheim (Erft) (Table 1). To put these factors into a larger statistical perspective, we calculated a similar peak factor for all gauges in the LUBW data set, but this time between the  $Q_{100}$  and all other return periods. In Table 2, for each return period both the mean and the maximum statistical peak factors from all 355 gauges are shown. The values in Table 2 thus provide a robust reference to broadly classify the 2021GD in terms of a few other return periods.

Even the smallest peak factor of 1.7 from Table 1 places the 2021 flood into the order of magnitude of a  $Q_{5000}$  to  $Q_{10\,000}$  compared to the mean, and  $Q_{500}$  to  $Q_{1000}$  compared to the maximum. The average peak factor of 3.3 (mean of all values in the PF column of Table 1) places the 2021 flood well beyond an  $Q_{10\,000}$ , both for mean and maximum. Similar to the comparison with the GRDC data, this underlines the exceptional nature of the 2021 flood. Finally, the maximum peak factor of

7.3 from Table 1 is so far beyond the peak factors in Table 2, and hence, so far beyond an  $HQ_{10\,000}$  that it raises doubts about the validity of evaluating the 2021 flood in terms of statistical return periods using short-run flow data. We will further investigate this matter in the next subsection.

### 505 3.2.3 Comparison to historical data

In this section, we focus on gauge Altenahr (river Ahr), which is selected for two reasons: first, it is placed in a region that is among the most severely affected by the 2021 flood (cf. PART1PART 1); second, long-term historical records are available for this gauge, which are helpful to illuminate the problem of estimating return periods of exceptional flood events.

Figure 7 shows the available flood events at gauge Altenahr. The events in orange are from the ten largest flood events in 510 the gauge recordings starting in 1946 and 1946. The gauge recordings from 1947 - 2016 were the basis for the  $HQ_{100}$  estimate ( $241\text{ m}^3\text{ s}^{-1}$ ) by the water administration of RP. The blue dots are historical floods, notably the 1804 and 1910 events, for which peak discharge estimates are provided by Roggenkamp and Herget (2014a), Roggenkamp and Herget (2014b), and Roggenkamp and Herget (2022). The red dots indicate the range of the 2021 flood peak estimated by the water authority of RP and the black crosses indicate the range of the 2021 flood peak estimated by Roggenkamp and Herget (2022) based on 515 gauge recordings and reconstructions. It is clearly visible that the gauge recordings since 1946 missed several major do not cover the entire range of the historical flood events, which renders the  $HQ_{100}$  based only on these values non-representative. Acknowledging this, the water authority of RP recently provided an updated  $HQ_{100}$  estimate of  $434\text{ m}^3\text{ s}^{-1}$  based on the entire time series from 1804 to 2021 (including the 2021 flood) as shown in Fig. 7 (Henrichs, 2022). Based on the updated  $HQ_{100}$ , the 520 peak factor for gauge Altenahr of the 2021 event reduces from approx. 4.0 (see Table 1) to approx. 2.3. Comparing the updated value to the values in Table 2 still places the 2021 event at Altenahr in the order of magnitude of an  $HQ_{10\,000}$  compared to the mean, and an  $HQ_{5000}$  to  $HQ_{10\,000}$  compared to the maximum.

With the purpose of showing the limitations of extreme value statistics based on non-representative samples, Vorogushyn et al. (2022) also estimated the return period of the 2021 flood at gauge Altenahr. While their estimated return period of the 2021 flood based on recorded data from 1949 to 2019 is larger than only, which means without considering the historical and 525 the 2021 floods. The resulting return period of over  $10^8$  years, which is very unrealistic and clearly shows the limitations of extreme value statistics for rare events based on non-representative samples. Including historical floods since 1804, the same authors then again estimated the return period of the 2021 flood to be in the order of magnitude of an  $HQ_{10\,000}$  and an, and the  $HQ_{100}$  of approx. to be about  $300\text{ m}^3\text{ s}^{-1}$  when adding historical floods since 1804. Comparing the corresponding peak factor of approx.. Note that the authors did not include the 2021 flood into their pool of events while Henrichs (2022) did, which 530 partly explains the differences between the two  $HQ_{100}$  estimates. Using the  $HQ_{100}$  estimate by Vorogushyn et al. (2022), the peak factor of the 2021 flood is about 3.0 with the values in Table 2 also places the event roughly into the order of magnitude of  $HQ_{10\,000}$ .

It is noteworthy that the authors report Vorogushyn et al. (2022) reported difficulties when fitting the a GEV distribution to the data and suggest the existence of a mixed rather than a single distribution, where the extreme floods of 1804, 1910, and 2021 535 come from a separate distribution. A possible explanation for such a mixed flood distribution could be the existence of rare

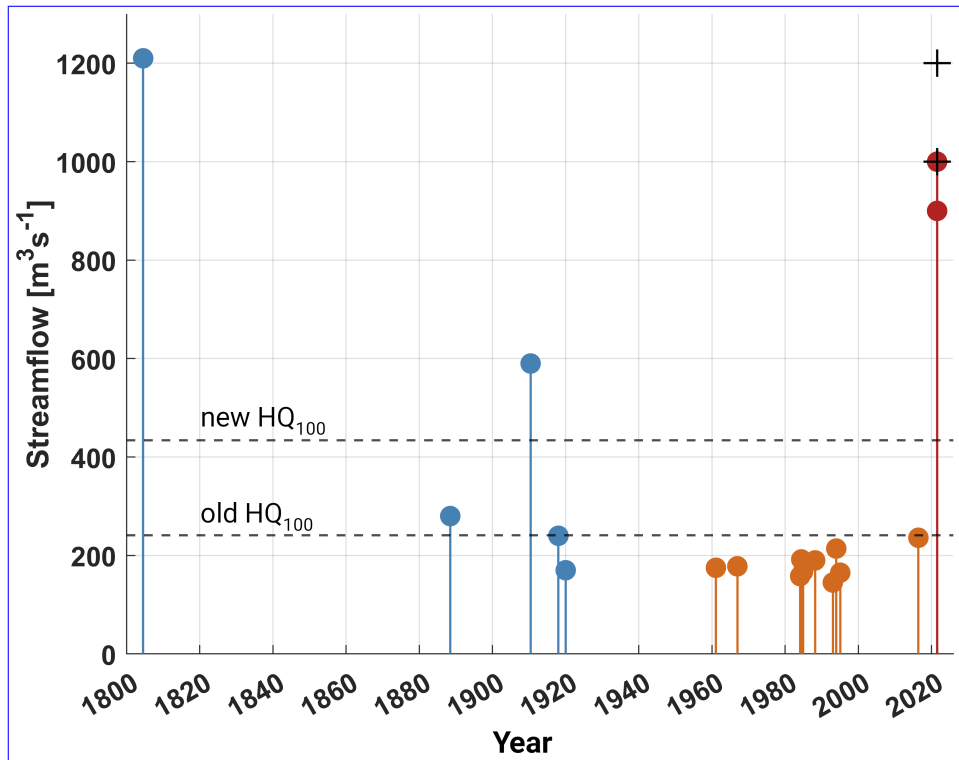


**Figure 7.** Time series of recorded and reconstructed selected flood peaks at gauge Altenahr (Ahr) (modified from Roggenkamp and Herget, 2022). The blue dots are reconstructions (modified from Roggenkamp and Herget, 2022); the orange dots are the 10 largest floods in the gauge recordings (starting 1946), provided by the water authority of Rhineland-Palatinate; the red dots indicate the range of the 2021 flood peak estimated by the water authority of Rhineland-Palatinate; the black crosses indicate the range of the 2021 flood peak estimated by Roggenkamp and Herget (2022) based on gauge recordings and reconstructions. The two dashed lines indicate the official  $HQ_{100}$  estimates using only instrumental recordings (since 1946; old  $HQ_{100} = 241 \text{ m}^3 \text{ s}^{-1}$ ) and a new approach including historical sources (new  $HQ_{100} = 434 \text{ m}^3 \text{ s}^{-1}$ ).

but extreme weather situations responsible for unusually large floods, and/or the onset of special rainfall-runoff mechanisms only in the case of extreme rainfall. One more Again, this underlines the challenges of extreme value statistics and the large uncertainties when estimating return periods for the 2021 event. It also indicates the need for even longer historical time series and reconstructions as far as possible, and/or the examination of the completeness of the events between 1804 and 1900–1946

540 as well as before 1804, where there is evidence that over 70 floods occurred in the Ahr River basin since the year 1500, including the large 1601 event (Seel, 1983). In addition, 1818 and 1848 were also large events with currently no reconstructed streamflows.

### 3.3 Hydro-morphodynamical perspective

In this section, we analyze hydrodynamic and morphodynamic processes which occurred in both, the Ahr and the Erft Valley, with the main focus on the following aspects that condition the downstream hazard: (i) the anthropogenic influence on the processes which evolved dramatically in hydro-morphodynamic processes in rivers that occurred in the last century, (ii) elements such as debris and sediments large debris and sediment which enhance the flood hazard, and (iii) the landscape organization and occupation which conditions the downstream hazard. landscape modifications due to urbanization. For the location of the discussed cases, we refer to maps given in PART 1, Figures 1 and 10.

The inclusion of sediment and linked geomorphic processes in the analysis of flood risk is discussed by several authors (e.g., Best et al., 2022). However, in the images taken in the aftermath of the July 2021 floods in Germany, it is striking to see that sediments contributed only a small portion to the total accumulated debris, which invaded the river network, streets, rural spaces, culverts, and buildings. There is an obvious and significant difference from similar images made one hundred or more years ago. The nature of the debris, which accumulates in narrower cross-sections in the urban space (streets) and river network (bridges), changed considerably. There is clearly an anthropogenic influence contributing to new types of debris of industrial origin. Besides sediments and the overwhelmingly present natural dead wood and vegetation, we observed a high volume of industrial elements such as vehicles and caravans, bins and containers, and construction materials, which exacerbated the hazard in the river systems.

We observed that parts of the Ahr Valley which historically would be occupied during flood events, and which often are preferential areas for deposition of sediments and debris transported by the flow, are now urban settlements. Such is the case of the southern part of the urban settlement of Schuld, which developed in the inner region of an Ahr Valley bend. This flow region is prone to sedimentation and a natural landscape sink of sediment and debris, which is transported by the river during floods. Parts of the town of Altenburg (Altenahr), bordering the right bank of the river Ahr, were constructed on an abandoned oxbow lake. The paleogeography of the valley shows that this region was an old meander of the river Ahr. Although dry under normal flow conditions, the abandoned oxbow lake is of alluvial nature and prone to inundation in high flow situations. Furthermore, being a low-velocity flow region, it is prone to sedimentation and settling of debris transported by the flood (Déprez et al., 2017). To a very limited extent, the inundation of this area may have contributed to the flow lamination and attenuation of the downstream peak discharge. Nevertheless, the main consequences of the inundation of this oxbow lake are negative, namely the destruction of the urban area settled herein as described in PART 1.

Another Regarding (i), an example of the consequences of the historical anthropogenic transformation of the morphology of the valley over time is the case of Dernau (cf. PART 1). As discussed in PART 1, the construction of a valley bottleneck increased substantially the flood levels recorded in July 2021 when compared to a similar flood in terms of peak the flood event with a similar discharge in 1804. In this particular case, we argue that morphological changes in the valley of anthropogenic origin may be the reason for more severe inundation levels during the 2021 flood event. This transformation was mainly materialized during the The changes in valley morphology due to the construction of the railroad (Ahrtalbahn) in the

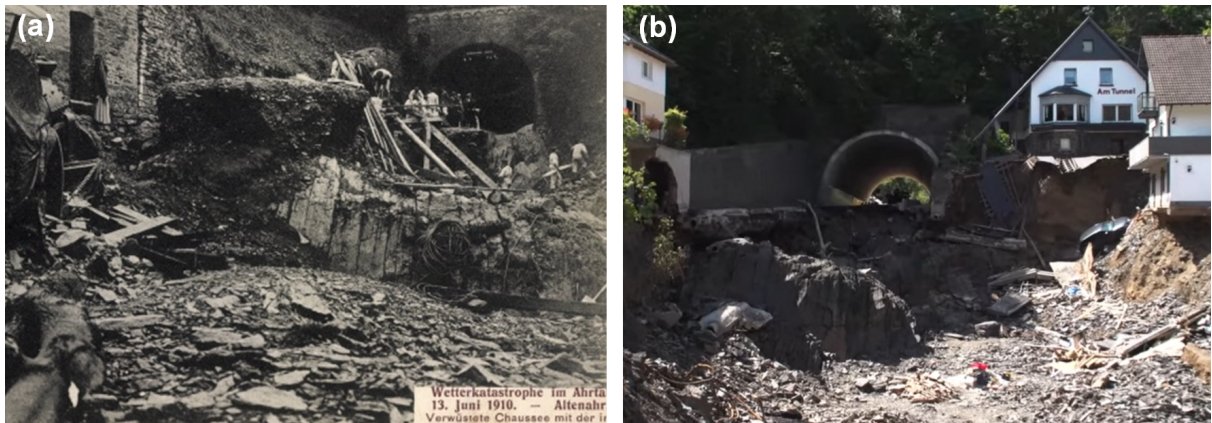


**Figure 8.** Downstream end of the road tunnel in Altenahr after (a) the flood of 1910 (photo credits: *Kreisarchiv Ahrweiler*), and (b) after the flood of 2021 (photo credits: Dieter Könnies).

1880s with several bridges that created ~~some bottlenecks downstream~~ bottlenecks downstream of the town of Dernau ~~— may be the reason for more severe inundation levels during the 2021 flood event.~~

As shown in PART I, the occurrence of a bypass in the landscape due to the ~~The~~ road tunnel in Altenahr (Ahr) is an cf. PART I) is another example of an anthropogenic ~~landscape singularity that disrupted the continuity~~ modification of the 580 valley ~~for extreme conditions as those in July 2021. In this case, the tunnel in Altenahr. It bypassed the flood through, which may have probably eliminated the lamination effect of one meander of the river Ahr. To which, to~~ a limited extent, ~~it is expected that~~ is expected to have increased the downstream peak discharge ~~was exacerbated. The main effect which is visible, however, must have been provoked by the substantial and sudden reduction of flow in the meander. Since the flood water was charged with sediments under suspension, substantial deposition when compared to the prior situation. However, the main observable~~ 585 ~~effect of the tunnel was the sediment deposition that occurred in the meander with the occurrence of the bypass changing considerably the channel morphology. The road tunnel in Altenahr bypassed meander due to the reduction of flow within it. This road tunnel~~ was constructed in 1834, and notably, the same flow bypassing happened already in the past during the 1910 ~~dramatic flood in the valley~~ flood (Fig. 8). The final configuration of the slope and ~~the~~ tunnel toe after the passage of both floods ~~show~~ shows striking similarities. An uncomfortable sensation of *déjà-vu* suggests the importance of considering 590 historical records and information in the preparation and planning for future flood events.

Besides bridges or tunnels, which are the most visible and paradigmatic historical changes of anthropogenic nature in the valley morphology, the construction of buildings, infrastructures, and industrial equipment add singularities to the landscape, which are capable of ~~dramatic~~ landscape alteration. Such ~~One example~~ was the case of the large-scale erosion episode that originated in the mining pit in Blessem (Erftstadt) in the Erft catchment. This mining pit, which was under exploration, ~~showed~~ 595 ~~to be a singularity in the landscape capable of triggering an impressive~~ triggered a large-scale process of retro-dendritic erosion. ~~The~~ A cavity formed due to this process caused the destruction of houses and endangered furthermore a ~~changing~~ change of the course of the river caused by the breach and collapse of the Erft riverbank that endangered the nearby highway. The occurrence

of such landscape changes, which have been spread in the territory over the last century needs further assessment. They can introduce local landscape fragility as the one in Blessem, but they can also be used as opportunities to retain flood volumes 600 having a positive effect on floods flood attenuation, as also happened in Blessem (cf. PART1 PART 1).

During the July Regarding (ii), the inclusion of sediment and linked geomorphological processes in the analysis of flood risk is discussed by several authors (e.g., Best et al., 2022). However, images of the July 2021 event, the destruction of gauging stations was particularly visible, for instance, in Altenahr (river Ahr). The destruction of these has negative consequences for flood management prior to and during emergencies since they are essential instrumentation to observe in real-time the 605 evolution of floods and to keep historical hydrometry records of the valley. The gauging stations are destructed by local scour or bank erosion and collapse. Analysis of the historical stability of the position, where they are placed, could inform a safer installation. Furthermore, the use of remote gauging in locations less susceptible to morphological changes during floods could be considered using videos (e.g., Le Coz et al., 2010), or other remote sensing techniques, to monitor hydrological quantities 610 in the rivers flood showed that sediments or natural dead wood and vegetation contributed only a small portion to the total accumulated debris, but that the nature of the debris changed considerably towards a high volume of industrial elements such as vehicles and caravans, bins and containers, and construction materials (cf. cover photo at RedaktionsNetzwerk Deutschland, 2022 “*Ein Jahr nach der Flutkatastrophe: So geht es den Menschen im Ahrtal.*”).

The hazardous effects of the meteo-hydrological extreme event herein described, ultimately depend on the landscape organization and occupation, and on the stability of the landscape and river morphology which is variable in time. Until 615 now, framework documents such as the Floods Directive (*Directive 2007/60/EC of the European Parliament and of the Council of 23 October 2007 on the assessment and management of flood risks*) are merely suggestive in the consideration of transported Regarding (iii), parts of the Ahr Valley, which historically would be occupied during flood events and which often are preferential areas for the deposition of sediments and debris in flood risk assessment. Consequently, the consideration 620 of moving boundaries and time-evolving hydro-morphodynamic processes in flood modeling and emergency planning is not common in Europe. Flood managers often consider a rigid landscape in flood risk assessment. Lane et al. (2007) argued on the need to consider the joint synergistic impacts of the combination of climate change and sediment imbalance in rivers, whereas Nones et al. (2017) explicitly defends the inclusion consideration of hydro-morphology and sediments in the implementation 625 of the Floods Directive. Lucía et al. (2018), who studied the 2016 flash flood in Braunsbach (Germany), suggested an update of the Floods Directive to require that flood risk assessment includes a heuristic hydro-morphodynamic approach, which considers the landscape and river channels network, transported by the flow, are now urban settlements. Such is the case of the southern part of the urban settlement of Schuld (see PART 1), which developed in the inner region of an Ahr Valley bend. This flow region is prone to sedimentation. Furthermore, parts of the town of Altenburg (Altenahr), bordering the right bank of the river Ahr, were constructed on an abandoned oxbow lake. Although dry under normal flow conditions, the abandoned oxbow lake is of alluvial nature and prone to inundation and deposition in high flow situations (Szymczak et al., 2022). The main 630 consequences of the inundation of this oxbow lake were the destruction of the urban area settled herein as described in PART 1.

## 4 Relation to climate change

In this chapter, we examine the 2021 flood in the context of future climate change. With this aim, it is of particular interest how a specific extreme event such as the July 2021 event would unfold under different climate conditions, and more generally, 635 what changes regarding the intensity and frequency of extreme precipitation events can be expected in the future. For the first, PGW simulations and subsequent hydrological discharge modeling were performed, and for the latter, conventional climate projections at the CPM scale (KIT-KLIWA) were considered in this study.

### 4.1 Pseudo-global-warming experiments

#### 4.1.1 The July 2021 precipitation event in a warming climate

640 Figure 9 shows the precipitation totals of PGW simulations of the July 2021 event against the background of different temperature perturbations. The control simulation (Fig. 9b) based on unperturbed ( $\pm 0.0\text{ K}$ , [hereafter PGWcontrol](#)) ERA5 initial and boundary conditions adequately reproduces the event in its magnitude and location (see also Fig. 1b for comparison). The simulated precipitation totals in LReg ([56.5 see Table mm d<sup>-1</sup>](#)) are [3](#) is almost equal to the observed totals ([55.4 estimated from RADOLAN data \(cf. PART mm d<sup>-1</sup> from RADOLAN; cfPART11\)](#)). Likewise, the most intense precipitation was simulated over the affected region. For SReg, the simulated precipitation totals ([88.5 mm d<sup>-1</sup>](#)) are slightly higher in comparison to the observed totals ([75.2 see Table mm d<sup>-1</sup> from RADOLAN3](#)). This overestimation might be due to a second simulated precipitation peak in the western part of SReg, which is not visible in the observations (see Fig. 1b).

645 Considering the PGW simulations, precipitation is lower under colder pre-industrial-like climate conditions ([e.g.,  \$-1\text{ K}\$ , hereafter PGWcold; Fig. 9d](#)) over LReg with a decrease of 11% ([50.3 Table mm d<sup>-1</sup> 3](#)), while warmer conditions ([e.g.,  \$+2\text{ K}\$ , corresponding to GWL3, hereafter PGWwarm; Fig. 9c, d](#)) lead to 18% higher precipitation totals over LReg([66.7 mm d<sup>-1</sup>](#)). Over SReg, the precipitation also decreases by 11% for [a  \$-1\text{ K}\$  cooling PGWcold](#), and increases by approx. 11% for [a  \$+2\text{ PGWwarm \(Table K warming3\)}\$](#) . Taking into account all PGW simulations (Fig. 9d, solid lines), the relationship between 650 temperature and [heavy](#) precipitation change follows indeed the Clausius-Clapeyron (CC) scaling (7% per 1 K) for the smaller SReg and even a super-CC scaling (9% per 1 K) for the larger LReg. This is in line with recent findings about the relationship between temperature and [heavy](#) precipitation, which found that daily precipitation extremes mostly increase at approximately the CC-rate (e.g., O’Gorman, 2015; Trenberth et al., 2003).

655 By [considering combining the](#) return periods based on the LAERTES-EU data (see Sect. 3.1.2, [Fig. 5](#)) and the PGW precipitation outputs, the change in the intensity of such an event under global warming can be assessed. For [SReg LReg \(SReg\)](#) the return period of [the control run is about 10 years. For  \$-1\text{ K}\$ , the return period is reduced to only 5 years, while for the  \$+2\text{ K}\$  simulation a return period of about PGWcontrol is about 20 years is estimated. For LReg, the differences in return periods became even higher. While for the control run, a return period of 20 years \(10 years can be assigned, the return period for the  \$+2\text{ K}\$  simulation increased to 200 years, emphasizing the hazardous potential of such an event in the context of future climate warming. This becomes even more evident when considering](#)) according to the LAERTES-EU data for data when considering the complete CReg area as reference (see Table 3)). Taking into account the LAERTES-EU data only for the LReg (SReg) only

665 (not shown). The (SReg) region, the return periods of the control run for these specific areas are around 100 to 150 years for LReg and 400 to 500 years for SReg. At  $-1\text{ K}$ , the return periods reduce to 50 to 60 years. PGWcontrol precipitation increases to about 100 years for LReg and 150 to 200 years for SReg, while for  $+2\text{ K}$  there is an increase to approx. 500 years (500 years for LReg and approx. 800 years) pointing out once again how special this event was for this particular region. Considering the precipitation totals from PGWcold leads to reduced return periods by a factor of about 0.5 for both LReg and SReg if this precipitation amounts would occur today (Table years for SReg. These are statistically rather robust estimates due to 3). The change in return periods is more pronounced for PGWwarm with an increase by a factor of 1.5 to 2 for SReg and by a factor of even 5 to 10 for LReg with respect to the total length of present-day LAERTES-EU statistics (Table 3). Thus, by assuming that such extreme events have the same frequency as today (equivalent with an identical return period) also in a warmer (or colder) climate, these results demonstrate that nowadays rare precipitation totals (with return periods of  $12T > 500$  years) will 670 become more extreme (corresponding to a present-day  $T > 200$  a event) due to climate change. However, possible changes in the frequency itself of such events are not investigated in this study.

**Table 3.** Spatially averaged 24-hour precipitation totals (14 July 2021, 06:00 UTC to 15 July 2021, 06:00 UTC) over the study areas (LReg and SReg) derived from RADOLAN observations  $\bar{R}_{\text{obs}}$  and from the PGW simulations  $\bar{R}_{\text{box}}$  (with box either LReg or SReg), and relative deviation  $\Delta_{\text{RR}}$  to the control run ( $\pm 0\text{ K}$ ); return period  $T$  of  $\bar{R}_{\text{box}}$  according to LAERTES-EU statistics considering either total CReg ( $T_{\text{CReg}}$ ) or only the two smaller study areas ( $T_{\text{box}}$  with subscript  $\text{box}$  standing either for LReg or SReg); peak discharge  $S$  from hydrological PGW simulations with LARSIM at gauge Altenahr (river Ahr) and from observations (reconstructions)  $S_{\text{obs}}$ , and relative deviation  $\Delta_S$  from the PGW results to the control run.

LReg						SReg			Altenahr (Ahr)		
	$-1\text{ K}$	$\pm 0\text{ K}$	$+2\text{ K}$	$-1\text{ K}$	$\pm 0\text{ K}$	$+2\text{ K}$		$-1\text{ K}$	$\pm 0\text{ K}$	$+2\text{ K}$	
$\bar{R}_{\text{obs}}$ (mm)		55.4			78.4				991		
$\bar{R}_{\text{box}}$ (mm)	50.3	56.5	66.7	79.1	88.5	98.4			650	801	1113
$\Delta_{\text{RR}}$ (in %)	-11		$\pm 18$	-11		$\pm 11$			-19		$\pm 39$
$T_{\text{CReg}}$ (a)	10	20	200	5	10	20					
$T_{\text{box}}$ (a)	50	100	500	200	500	800					

#### 4.1.2 Hydrological response

The first test with LARSIM-Ahr using the original PGW precipitation fields revealed a mismatch and non-conclusive results for the resulting peak flows (not shown) due to slight spatial shifts of the rainfall centers between the scenarios. The resulting rainfall totals in the rather small ( $749\text{ km}^2$ ) Ahr river basin did not reflect the overall areal rainfall decrease or increase of the PGW scenarios. To overcome this shortcoming, a more robust approach is applied determining In order to explicitly elaborate the pure hydrological response to a changed precipitation intensity, we determine correction factors for the two considered PGW scenarios  $-1\text{ K}$  (PGWcold) and  $+2\text{ K}$  (PGWwarm) compared to the PGW control simulation (PGWcontrol,  $\pm 0\text{ K}$ ) PGWcold and PGWwarm compared to PGWcontrol instead of using the simulated spatial precipitation fields. As

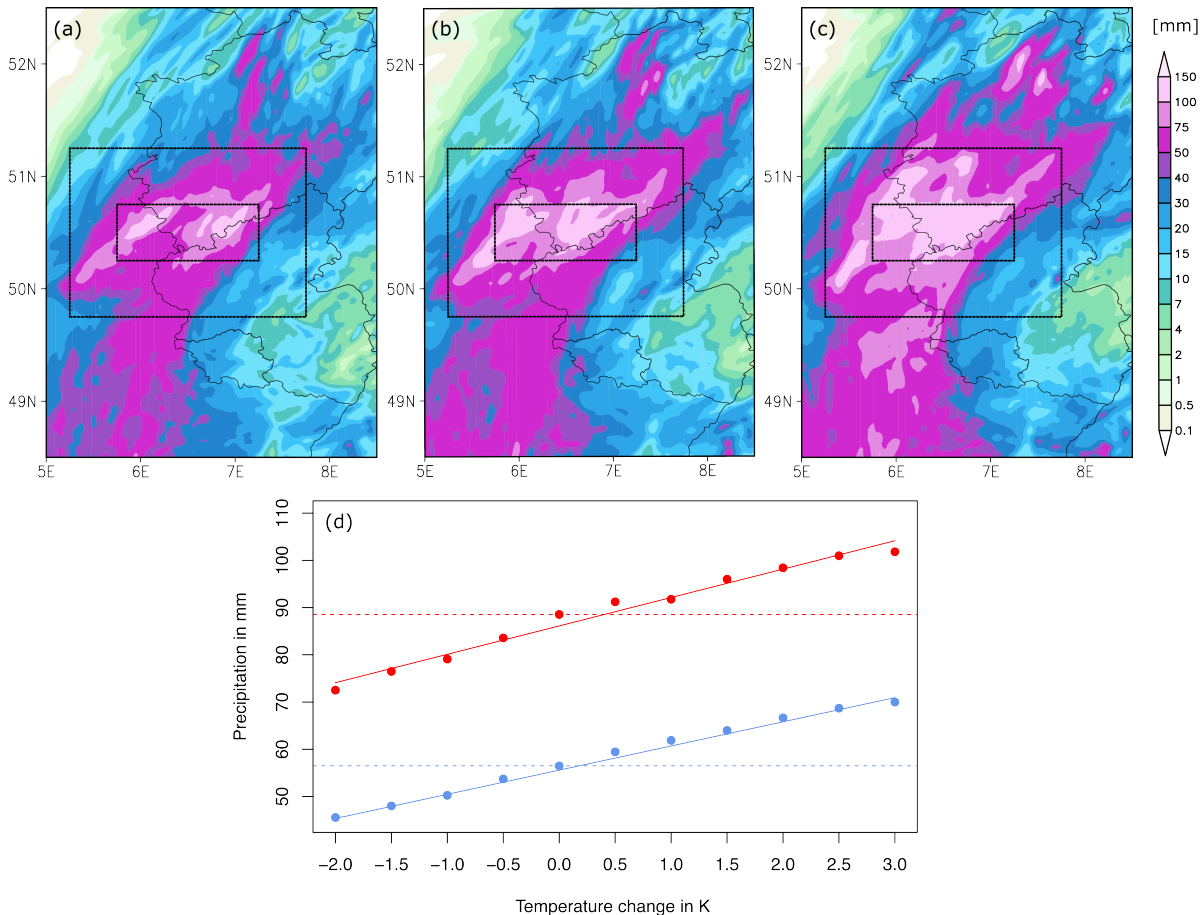


**Figure 9.** 24-hour precipitation sums (14 July 2021, 06:00 UTC to 15 July 2021, 06:00 UTC) from PGW experiments using the WRF model. Horizontal distributions for (a) PGW  $-1\text{ K}$  ([PGWcold](#)), (b) control run  $\pm 0\text{ K}$  ([PGWcontrol](#)), and (c) PGW  $+2\text{ K}$  ([PGWwarm](#)). (d) Area averaged 24-hour precipitation sums (LReg in blue, SReg in red) plotted against temperature change for all conducted PGW experiments. Solid lines represent linear regression lines that are used for calculating the correction factors for the hydrological discharge modeling (see Sect. 4.1.2). Stippled horizontal lines denote the mean 24-hour precipitation amount of [the control run PGWcontrol](#) (56.5 mm for LReg, and [88.688.5](#) mm for SReg).

685 demonstrated in the previous section, the spatially averaged rainfall totals for LReg of PGWcontrol match the observed totals from RADOLAN. Using the derived linear regression function for LReg (Fig. 9d, solid blue line), the ratios between the PG-  
 690 Wcontrol and the scenarios PGWcold (PGWwarm) were calculated. The resulting adjustment factors were 0.92 for PGWcold, and 1.16 for PGWwarm representing the climate change signal compared to present-day conditions. The observed rainfall data set used for the LARSIM-Ahr reference simulation was then multiplied by these factors and used as input for two additional LARSIM-Ahr scenario simulations.

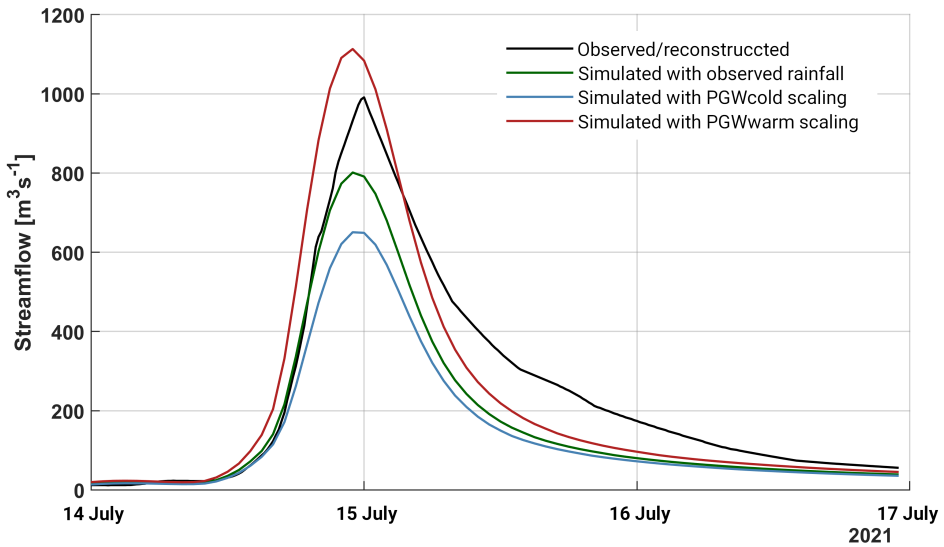


**Figure 10.** Streamflow at gauge Altenahr (Ahr). Black is from observation and reconstruction (cf. [PART1](#)[PART1](#)), green is from LARSIM-Ahr simulation forced with observed rainfall (Bardossy et al., 2022), blue is from simulation with PGWcold rainfall scaling, and red is from simulation with PGWwarm rainfall scaling.

Figure 10 shows observed and simulated streamflow time series at gauge Altenahr (Ahr). The black line shows the values based on observation and reconstruction (cf. [PART1](#)[PART1](#) for details), the peak value of  $991 \text{ m}^3 \text{ s}^{-1}$  (see also Table 3) corresponds to the upper red dot in Figure 7. The green line shows the simulated streamflow time series using LARSIM Ahr with the best available rainfall observation product as input. The corresponding peak flow ~~of  $801 \text{ m}^3 \text{ s}^{-1}$~~  underestimates the observed one by about 20 % (Table 3). This can be attributed to deficiencies in the hydrological model, the initial conditions, and the used rainfall product. Nevertheless, the overall magnitude and course of the event are well captured. The blue and red lines show the results of the streamflow simulations based on the observed rainfall scaled by the ratios of PGWcontrol to PGWcold and PGWcontrol to PGWwarm, respectively. The resulting simulated peak flows ~~of  $650 \text{ m}^3 \text{ s}^{-1}$  (PGWcold)~~ and  ~~$1113 \text{ m}^3 \text{ s}^{-1}$  (PGWwarm)~~ are smaller (larger) than the reference by a factor of 0.81 (1.39). For both the cooling and the warming scenario, the hydrological response was, therefore, more pronounced than the meteorological one. For PGWcold, a precipitation decrease of 11 % was simulated while the LARSIM-Ahr simulations show a decrease of the flood peak of 19 %. This non-linear response is even more pronounced for PGWwarm, where a precipitation increase of 18 % for LReg caused a 39 % increase in the flood peak. This indicates that increasing meteorological hazards due to climate change may be amplified by the rainfall-runoff transformation.

#### 705 4.2 [High-resolution](#) future climate projections

The evolution of heavy precipitation in a warming climate is now investigated in conventional climate projections using the KIT-KLIWA ensemble considering exemplary the 10-year return [value](#) ([RV10](#)) of spatially averaged daily

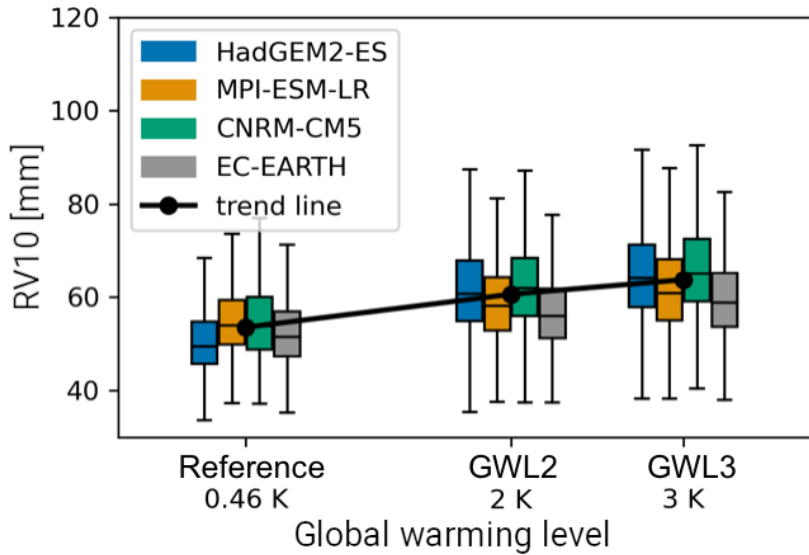


**Figure 11.** Box plots of spatially averaged [RV10-RL10](#) distributions over CReg for the reference period, GWL2, and GWL3 for all ensemble members of KIT-KLIWA. The boxes represent the lower and upper quartiles, the center lines the median, and the whiskers outliers, defined as more than 1.5 times the interquartile range. Black dots and line show the multi-model ensemble mean for each set of runs and the trend.

precipitation. Figure 11 shows the development of [RV10-RL10](#) with ongoing global warming for each of the four ensemble members for CReg. The distribution of return [values-levels](#) within CReg is represented in the box plots. For the reference period (1971 to 2000; equivalent to GWL of +0.46 K compared to pre-industrial conditions), the [RV10-RL10](#) averaged over CReg is 54.0 mm for the ensemble mean (Fig. 11, black dots and line).

710 For comparison, the [RV10-in-KOSTRA](#) (cf. [PART1](#) and [Malitz and Ertel, 2015](#)) [RL10 in KOSTRA](#) (cf. [PART 1](#) and [Malitz and Ertel, 2015](#)) averaged over the German part of CReg is 64.0 mm, so the KIT-KLIWA result is about 10 mm (or 18 %) smaller. However, the model-based value was calculated for fixed calendar days, whereas KOSTRA gives the maximum precipitation in an arbitrary 24-hour interval. The 715 German regulations *DWA-Regelwerk 531*, which KOSTRA is based on, proposes a factor of 1.14 to correct this methodical difference. Applying this technical correction to the KIT-KLIWA data, the adjusted [RV10-RL10](#) is 61.6 mm (4 % difference to KOSTRA). Furthermore, Junghänel et al. (2017) specified a uncertainty range of  $\pm 15\%$  for a 10-year return [interval-period](#) in KOSTRA. Taking both into account, the KIT-KLIWA data are in the range of KOSTRA.

720 For each ensemble member, the average value increases with proceeding global warming (Fig. 11). The extent of this increase measured as the normalized difference between GWL3 and reference period varies slightly between the simulations with the strongest (lowest) increase in the CNRM-CM5 (EC-EARTH) driven simulation. Averaging over CReg and all ensemble members, a trend of 4 mm per degree of warming is predicted. This corresponds to a relative change of 8.4 %. Considering the LReg only, the increase is about the same magnitude with 7.8 %, and also the individual ensemble members show similar behavior (not shown).

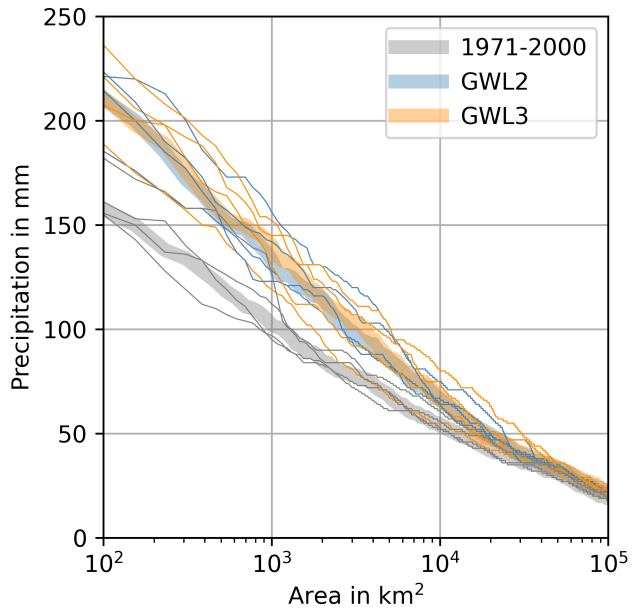


**Figure 12.** Spatial extent of daily precipitation clusters (contiguous grid points) above the ~~RV10 RL10~~ estimated from the KIT-KLIWA data set for the present-day reference period, GWL2, and GWL3. Thin lines represent individual ensemble members, and thick lines the ensemble mean.

725 The analysis of additional return ~~values~~ ~~levels~~ showed that the magnitude of the relative increase per degree of warming depends on the return period with lower (higher) rates ~~in the mean~~ for shorter (longer) return periods (Table S3). For CReg, the increase between the reference period and GWL3 is only 5.6 % for the 1-year return ~~interval~~<sup>period</sup>, and 7.5 % for the 5-year return ~~interval~~<sup>period</sup>. For longer return periods (e.g., 30 years), the relative increase is higher with 10.1 % per degree of warming. Thus, the scaling of heavy precipitation with global warming is projected to be in the range of the Clausius-  
 730 Clapeyron scaling (7 % per 1 K warming) for return periods of 3 to 10 years. ~~For LReg, the climate change signal is about 0.5 to 1.0 % per degree warming smaller than for CReg for all considered return periods.~~ Analysis showed that this increase is not purely linear, but a slightly stronger increase is observed when considering the change from the reference period to GWL2 only (Table S3). However, the ~~deviation from the linear trend is within the large range of variability of the ensemble uncertainty of these estimates, indicated by the ensemble interquartile spread (25th to 75th percentile; Table S3) also increases with the return~~  
 735 ~~periods due to the decreasing amount of events taken into account. Within the ensemble spread, CReg and LReg show similar change signals.~~

As already elaborated at the beginning of the paper, the severity of a precipitation event depends not exclusively on the local intensities. The affected area is another essential factor especially for triggering floods. Analogous to ~~the analyses in~~ Sect.3.1.2 ~~based on the LAERTES-EU data set~~, a cluster analysis was conducted for the KIT-KLIWA ~~simulations~~ to investigate

740 the development of the spatial extent of **RV10-RL10** in a warmer future. **Therefore, the affected area of daily precipitation events was determined over the contiguous grid cells exceeding a certain precipitation threshold for the ensemble reference 1971 to 2000, GWL2, and GWL3.** As in Sect.3.1.2, the return level was derived from the occurrence to display RL10 (3 occurrences per 30-year time slice) in Fig. 12.

745 The projections show that the extent of precipitation loads experienced today as an **RV10-RL10** will increase in a warmer climate (Fig. 12). The analysis of the single ensemble members (thin lines in Fig. 12) shows that all four members as well as the ensemble mean (thick lines in Fig. 12) agree on the increase of larger events in a warmer climate. However, though the difference from the reference period to GWL2 is clearly visible, only a few changes are projected on average from GWL2 to GWL3. The small spread between the ensemble members in the reference period, especially for large areas (more than 1000 km<sup>2</sup>), increases at GWL2 and GWL3. **The relative increase is almost constant for a wide range of areal dimensions of contiguous clusters. For example, a cluster with daily precipitation totals of at least 150 mm nowadays occurs at an extent of about 150 km<sup>2</sup> while such an event is expected to extend about 600 km<sup>2</sup> for GWL2 and GWL3. The present-day intensity of a cluster of 600 km<sup>2</sup> is about 115 mm; the future intensity for a cluster of 150 km<sup>2</sup> is about 200 mm, which in both cases is an increase of about 30 %.** Primarily and as described above, the changes in the affected area are attributed to the general increase in extreme precipitation in a warmer climate as a higher specific humidity is anticipated under warmer conditions. This results 750 in larger clusters of high rainfall totals that multiply the amounts of water available as runoff in downstream valleys. The size of those clusters is thus crucially responsible for the impact of an event. Therefore, the analysis of rainfall events beyond solely the intensity but with the inclusion of the extent is crucial for the impact of an event. With similar intensity, more expanded events tend to cause larger flooding. For areas larger than 20 000 km<sup>2</sup> no changes can be resolved by the analysis anymore, which is also influenced by the limited area of the model domain, bounding these large extreme events.

760 The results presented above indicate that the projected precipitation change for high return **values-levels** might even exceed the theoretical CC-scaling (super-CC scaling) over **the** south and central Germany in a warming climate. Comparing the results with the PGW simulations for the July 2021 event (see Sect. 4.1.1), the relative changes within the conventional climate projections of KIT-KLIWA are of similar magnitudes. In comparison with the **RV10-RL10** in LAERTES-EU (Fig. 5), the **RV10-RL10** in KIT-KLIWA is smaller by about 30 % over the entire range of analyzed spatial dimensions. This discrepancy might largely 765 be attributed to the difference in ensemble size (factor 10) and a varying bias correction. Additional uncertainties arise from different methods of estimating the **RV10-RL10** (GPD in the case of KIT-KLIWA and empirical in the case of LAERTES-EU).

#### 4.3 **Further considerations Hydro-morphodynamic responses on flood management under a changing climate change**

770 **Harrison et al. (2019) concluded that different landscape settings respond differently to changes in climate. Consequently, the evaluation of the effects of global warming on flood hazards is not restrained to considerations of extreme meteorological events. The physical processes causing flood hazards are a combination of extreme meteorological events with the As climate determines the landscape occupation and organization and with the stability of the landscape and river morphology. These factors, together with the societal response to emergencies, define the level of flood hazard of a valley.**

775 Climate conditions the landscape occupation and organization, so it is expected that global warming will cause changes in the land cover due to the adaptation of natural elements such as vegetation and soil. Furthermore, it will force the adaptation of human activities and soil use, for instance, by adaptation of agricultural practices. These factors, in turn, have a direct effect on the surface flow, and on the influx of inorganic sediment (Eekhout and de Vente, 2022) and large debris such as deadwood. Rivers are dynamic systems, where non-linear interactions occur between the flowing water, the boundaries, which can be erodible or fixed, moving sediment, and debris and vegetation (Seminara, 2010). (Eekhout and de Vente, 2022). Imbalances in river systems, for instance, such as changes in discharge, riverine aquatic and riparian vegetation, and sediment production can have dramatic effects on the fluvial morphology stability and riverine vegetation can have impacts on fluvial morphology and flow conveyance (Crosato et al., 2022). These aspects are all vulnerable to climate change.

780 As seen in the analysis of the July 2021 extreme floods, this dynamic character of valleys and rivers ultimately impacts the flood hazard. The non-linear interactions and morphological changes are a permanence in rivers occurring at these different time scales. Beaty (1974) and Kern (2013) conceptualized a division of flow events in rivers between those corresponding to equilibrium processes and those corresponding to, what they call, catastrophic processes, those that represent dramatic changes in the river morphology. The second type of event is the one scarring the landscape and river channel networks, changing the boundaries with which static flood modeling is commonly done. Long-term channel bank and slope adjustments correspond to long-enough periods during which one may assume steadiness in channel morphology (several decades) and are easily incorporated by a classical flood risk analysis based on fixed boundaries. Mid-term reach adjustments, happen in a multi-year time scale typical inferior to the return period which is considered on flood risk assessment (see discussion by Bung (2021) based on the current extreme events), hence requiring at least the analysis of the sensitivity of flood modeling results to morphological changes in flood risk assessment (Pender et al., 2016; Radice et al., 2016). Short-term local-to-reach adjustments occur almost instantly or on a timescale corresponding to the duration of the flood event (minutes to days), for which the consideration of dynamic changes of river morphology during events is necessary (Dietze and Ozturk, 2021).  
785 Considering the frequency of occurrence, Furthermore, Magilligan et al. (1998) argued that the frequency of occurrence of flood events and river morphological adjustments may not always coincide. The channel-forming flow in a river typically corresponds to a hydrological flood with a return period of 1 to 10 years (Copeland et al., 2000; Doyle et al., 2007; Annable et al., 2011), depending on many other factors such as landscape occupation, slope, valley confinement, stream power-flood period and sequence (e.g., Magilligan et al., 1998; Lueia et al., 2018). These two important factors for flood hazard evaluation and implementation of flood mitigation measures, frequency, are the frequency and duration of extreme events. Both are susceptible to climate change bringing hence global warming, hence bringing extra complexity for flood managers.

800 Taking a historical perspective, there are two main aspects that influence the flood hazard in valleys, which are important to highlight: the time-varying character of the valleys, which happens at scales that are not necessarily compatible with the return periods considered for flood management, and the anthropogenic changes in valleys, which, besides being responsible for the urban occupation, have a direct influence in channels morphology and an indirect influence on the type of debris reaching the rivers. These two aspects correspond to a twofold intersection with climate change: the changes that climate scenarios may have on landscape and river morphodynamics (uncertain weathering and alteration in land cover) are still to be unraveled.

Finally, in a context of an uncertain and changing climate, a probabilistic analysis of the combination of landscape oddities, as some herein described, with extreme meteorological events is necessary to stress test the safety of valleys against improbable 810 and unforeseen occurrences such as the ones occurred in July 2021 in Germany.

## 5 Discussion and conclusions

The present work is the second part of an interdisciplinary study describing, analyzing, and classifying the disastrous July 2021 precipitation and flood event in Central Europe mainly affecting western Germany with the Ahr and Erft river basins. The main focus of the second part was on (i) the comparison and classification of this event in a historical and statistical context and (ii) 815 the assessment of future climate change effects on such extreme events. Both aspects were investigated under a meteorological, hydrological, and hydro-morphological perspective. The main conclusions with respect to the research questions from Sect. 1 are as follows:

(I) How does the event classify within the historical context of precipitation and flood events?

The July Different metrics used to classify the July 2021 precipitation event in the historical context considering intensity, duration, and extent revealed that it was among the most intense historical precipitation events in the past 70 years in Germany (ranked 5th). However, the statistical analyses using the LAERTES-EU RCM ensemble revealed an underestimation of return values derived using observational records given their limited length. The observed discharges of the July 2021 flood event along the river Ahr were extreme regarding statistics based on observations, but not extraordinary when additionally considering reconstructed historical events (e.g., 1804, 1910), demonstrating that the existing flood hazard maps at the time did 820 not represent the actual flood hazard. In which way did the historical transformation of river valleys (e.g., landscape occupation and organization) change the 2021 flood hazard in comparison to past events in this region? The cases of the municipalities Sehuld and Altenahr (river Ahr) showed that in order to improve flood management practices, it is crucial to better understand the historical land use of the valley such as the reactivation and inundation of the abandoned oxbow lake in Altenburg (Altenahr), which has been urbanized over time. The comparison of the 2021 flood with past events revealed the importance 825 of considering the anthropogenic or natural transformation of the landscape and valleys for flood management. The inclusion of sediments and debris in flood modeling is essential, including new types of industrial large debris, which did not exist in the historical floods analyzed. How would the July 2021 precipitation event unfold under different past and future climate conditions and what implications have these scenarios on flood events? A further intensification of such events (both regarding precipitation and resulting floods) is expected with ongoing global warming. Using a series of PGW simulations representing 830 different levels of global warming, the results showed that the precipitation intensity increases in the order of the theoretical Clausius-Clapeyron (CC) scaling with 7 to 9 according to  $HPE_{crit}$ . Our analyses also revealed that the July % per degree warming. The present-day control run already showed an increase of about 11 % in intensity compared to pre-industrial-like conditions, which is equivalent to a doubling of the statistical probability of occurrence. Using the PGW simulations as input for a hydrological model revealed strong non-linear impacts on the hydrological response beyond the CC-scaling. How are 835 precipitation characteristics (e.g., intensity, extent) projected to change under future climate conditions? The high-resolution 840

future KIT-KLIWA ensemble also confirms the CC scaling for the mean and moderate intensities. For more intense precipitation, however, the analyses revealed a super-CC scaling of more than 10 % per degree warming. This implies further intensification of heavy precipitation. Moreover, the area affected by a specific intensity level is expected to grow.

Regarding conclusion (I), different metrics used to classify the July 2021 precipitation event in the historical context 845 considering intensity, duration, and extent revealed that it was among the strongest events in Germany but not unique. precipitation event was unique concerning its location in western Germany, while the majority of the other extracted extreme precipitation events occurred in eastern or southern Germany with some regions being affected by multiple events. The shape and the position of the precipitation areas of these events are emerging from quasi-stationary low-pressure areas over southern or 850 eastern Central Europe (e.g., Stucki et al., 2012; Kelemen et al., 2016) and are latter event sample are often associated with a Vb cyclone pathway. This setup mainly favors, which is known to favor the occurrence of extremes extreme precipitation in eastern and southern Germany, thus, the July (e.g., Stucki et al., 2012; Kelemen et al., 2016). In contrast, for the July 2021 event in western Germany is an exception. Nevertheless, our analyses revealed that the July 2021 precipitation event was less unique in a broader historical and climatological context. Wet soils and local moisture recycling do not seem to be major factors in preconditioning and feeding the event. Here, large-scale mechanisms and the advection of moisture from remote 855 sources were the driving factors (cf. PART1). This was for example, for example, also the case in the 29 June 2017 event (Caldas-Alvarez et al., 2022a), where even higher precipitation totals were registered. Nevertheless, the Wet soils and local moisture recycling do not seem to be major factors in preconditioning and feeding the event. The presented results are in line with Schröter et al. (2015), who also found no observed flood-triggering heavy precipitation events on top of a very wet period in the used observations. However, the statistical analyses using the LAERTES-EU RCM ensemble revealed 860 an overestimation of return periods derived using observational records given their limited length. Considering the larger CReg domain, the July 2021 event has a return period according to LAERTES-EU of about 10 to 20 years. The derived return periods increase to 100 to 200 years when considering only data for LReg (SReg). Comparing these results to the findings in PART 1 or Kreienkamp et al. (2021), who both estimated return periods for the event of several hundred to 1000 years based on observations clearly highlights the uncertainty of a return period estimation solely based on such (short-termed) data sets or 865 for specific areas. Although exceptional for that particular region, comparable precipitation events occur more frequently in a statistical sense anywhere within CReg.

From the hydrological perspective, the July 2021 flood event was exceptional, when (i) compared to long-term gauge recordings from a large region with a similar hydroclimate (CReg; GRDC data), (ii) compared to statistical return periods derived from a large set of gauges (LUBW data), and (iii) when compared to long-term historical records at gauge Altenahr (Ahr).

870 While events in the order of magnitude of the 2021 flood were already observed at gauge Altenahr in the past (e.g., 1804, 1910), robust estimation of statistical return periods proved to be difficult and afflicted with large uncertainties. Along both the Ahr and Erft River Rivers, the 2021 event exceeded the statistical 100-year return value level ( $HQ_{100}$ ) by a factor of up to 7, which is so far beyond observed gauge records that a return period estimation is questionable to impossible. The July This also demonstrates that the existing official flood hazard maps at the time did not represent the actual flood hazard. The July 2021 875 flood event, therefore, should be seen as a wake-up call to include additional information as much as possible in the risk assess-

ment and estimation of hydrological and hydraulic design values rather than relying mainly on extreme value statistics based on gauge recordings with limited time coverage. Further, the results suggest that the range of extrapolation when estimating rare floods from limited observations should be chosen conservatively, especially under the non-stationary conditions imposed by climate change. Such additional information could be reconstructed from historical floods or hydrological simulations forced by long-term climate simulations including the effects of climate change as boundary conditions.

880 (II) In which way did the historical transformation of river valleys (e.g., landscape occupation and organization) change the 2021 flood hazard in comparison to past events in this region?

In terms of hydro-morphodynamic processes (conclusion II), the analysis of historical events indicated that the current methods for the evaluation of ~~flood hazards~~ the flood hazard do not capture or account for changes in the hydro-morphology of 885 river networks such as landscape organization and occupation. These historical changes include also the influence of human activities as constructors of the landscape and river morphology, a role which was considerably intensified in the last century. The ~~consideration of the history of the landscape~~ cases of the municipalities Schuld and Altenahr (both along the river Ahr) showed that in order to improve flood management practices, it is crucial to better understand the historical land use of the 890 valley. These considerations (based on images and reports and on paleogeography investigation) ~~reveals~~ revealed additional areas prone to inundation or damage by sediment and debris, such as the abandoned oxbow lake in Altenburg (Altenahr) or the Ahr River bend in Schuld. ~~Furthermore,~~ which both had been urbanized over time. Until now, framework documents such as the Floods Directive (Directive 2007/60/EC of the European Parliament and of the Council of 23 October 2007 on the assessment and management of flood risks) are merely suggestive in the consideration of transported sediments and debris in flood risk assessment. Cases like the July 2021 floods showed that the consideration of sediments and large debris 895 including new types of industrial large debris, which did not exist in the historical floods analyzed, and the consideration of sediments and large debris and associated geomorphological processes in flood modeling, is essential to fully capture the flood hazard (Dietze et al., 2022) (Nones et al., 2017; Lucía et al., 2018; Dietze et al., 2022; Best et al., 2022). Several natural and anthropogenic aspects that condition the evolution of the landscape are climate-driven as well, which means that the determination of flood hazards and risk is a highly complex task in the context of global warming.

900 Regarding conclusion (III) How would the specific extreme event of July 2021 unfold under different past and future climatic conditions and what implications do these scenarios have on flood events?

A further intensification of similar events (both regarding precipitation and resulting floods) is expected with ongoing global warming. Therefore, the July 2021 event was re-simulated with the WRF model using a series of PGW simulations, representing 905 different levels of global warming by altering the mean temperature state from -2 K to +43 K and keeping the relative humidity constant. This storyline approach was used here to complement the probabilistic approach of analyzing huge ensembles of climate model data to represent uncertainties in physical aspects of climate change on specific events (Shepherd et al., 2018). The control run ( $\pm 0$  K) uses the present-day conditions, which represent a global warming level of already +1.09 K (GWL1) according to IPCC (2022). It could be demonstrated that the event precipitation follows ~~the theoretical a (super)~~ CC-scaling of 910 about 7 to 9 % increase per degree warming, which is in line with findings by Trenberth et al. (2003) or O’Gorman (2015). A higher CC-scaling precipitation scaling is found for the larger LRegLReg, underlining the unusual nature of the July 2021 event

in terms of its spatial extent. The present-day control run already showed an increase of about 11 % in intensity compared to pre-industrial-like conditions (GWL0), showing that the increase in precipitation does not always have to follow CC-scaling. Putting the spatial mean precipitation from the PGW simulations PGWcold and the present-day climate conditions into the statistical context of LAERTES-EU, the (for both the entire CReg domain and the specific LReg/SReg domains), the simulated 915 increase in precipitation is equivalent to a doubling an increase of the return period for both LReg and SReg from 5 to 10 years, which is equivalent to a doubling in the probability of occurrence compared to pre-industrial-like conditions by a factor of 2 to 2.5 if both precipitation totals would occur today. The +2 K simulation predicts an a further increase in precipitation of 11 % for SReg, which means a further doubling increase of the return period to 20 years again by a factor of 1.6 to 2. For LReg, an increase of 18 % is simulated leading to a dramatic increase of in the return period to 200 years by a factor of 5 to 10.

920 Using the PGW simulations as input for a hydrological model revealed strong non-linear impacts on the hydrological response beyond the CC-scaling. For gauge Altenahr (Ahr), the PGWwarm (PGWcold) scenario with an 18 % increase (11 % decrease) of rainfall led to a 39 % increase (19 % decrease) of the flood peak. This emphasizes the that in addition to the rainfall-amplifying effect of CC-scaling, the non-linear relationship between meteorological drivers and hydrological response with the hydrological response has the potential to further magnify hazards related to climate change along the meteorological-925 hydrological-morphological process chain. Investigating in further detail the hydrological reasons for this amplifying effect (e.g., an increase of fast surface runoff) is beyond the scope of this work, but a relevant topic for further research, especially, as such effects should not be specific to the Eifel region in western Germany and the 2021 flood event, but broadly apply to many catchments around the world.

930 Regarding conclusion (IV), the (IV) How are precipitation characteristics (e.g., intensity, extent, frequency) projected to change in general under future climate conditions?

The convection-permitting ensemble simulations of KIT-KLIWA over the study area agree on an intensification of extreme precipitation in a warmer climate. Precipitation at a given return period increases across all duration levels studied. The analyses confirm confirmed an increase in moderate precipitation intensities following the CC-scaling, but also indicate but also indicated an intensification above the CC-scaling (super-CC scaling) of more than 10 % per degree warming for the highest 935 return periods consistent with Feldmann et al. (2013) or Lenderink et al. (2021). Furthermore, the spatial extent of events, meaning the area affected by a specific intensity level, is expected to grow. Both trends lead to a general increase in the probability that a location is affected by precipitation extremes. Especially for sensitive areas, such as the steep terrain along the Ahr Valley, or generally, the accumulated effect of such extreme events along river reaches, we thus expect an increased hazard potential in a warmer climate. However, the results show no clear signal regarding the frequency of extreme events. Moreover, 940 the study is limited by the number of 30 simulation years for each of the four ensemble members, leading to large uncertainty with increasing return intervals periods. Therefore, further analyses with more data (e.g., from initiatives like the Coordinated Downscaling Experiment (CORDEX) of the World Climate Research Program) are needed.

To summarize, precipitation, especially heavy precipitation, remains a challenging task for both observational analyses and statistics, as well as for model simulations and future projections research topic (cf. Stocker (2014); ?). Observational 945 Stocker (2014); IPCC (2021a); observational records in most cases are still too short to fully capture the intensity and fre-

quency of extremes that are ~~basically physically~~ possible. Synthetically extending these records with model simulations also has limitations due to the complexity of precipitation formation, which leads to distinct biases in the simulations. These shortcomings directly propagate into hydrological models and resulting discharge statistics such as the HQ<sub>100</sub>. Furthermore, discharge records are likewise available for short periods only, requiring statistical extrapolations for higher return periods with 950 related uncertainties. However, official guidelines and regulations for flood risk assessments and mitigation rely solely on these observation-based metrics. The presented analysis could show to some extent that consideration of historical records ~~such as photos or written chronicles~~ in the reconstruction of past flood events can reduce the uncertainty of metrics such as the HQ<sub>100</sub>. The general inclusion of such sources would significantly improve the evaluation of the potential hazard. Within the scope of ongoing climate change and the expected further increasing precipitation intensities, this becomes increasingly relevant. 955 Another complement is the forcing of the existing hydrological water balance models with precipitation data from the high-resolution future scenarios to investigate probable future changes in discharge statistics, which can then be used for mitigation purposes. With the recently ongoing development in climate research towards higher-resolution, convection-permitting simulations in the near future (e.g., within the BMBF project “NUKLEUS” for Germany), it is expected that the ~~precipitation statistics estimation of future precipitation statistics and its spatial representation~~ will become more robust. ~~We anticipate that 960 this will increase the potential for spatial information to be better represented.~~

*Data availability.* HYRAS-DE, RADOLAN, and KOSTRA are freely available for research at the Open Data Portal of the German Weather Service DWD (<https://opendata.dwd.de>, last access: 8 June 2022). HYRAS data can be requested at DWD for research and education purposes. Gauging data are provided by the Global Runoff Data Centre (GRDC) and are freely available at the GRDC portal (<https://www.bafg.de/GRDC/>, last access 22 May 2022). Regionalized flood information for Baden-Württemberg (BW-Abfluss) is freely available at the LUBW 965 portal (<https://udo.lubw.baden-wuerttemberg.de/projekte/>, last access 22 May 2022). River gauge data are available on request from the responsible water authority: Water administration of Rhineland-Palatinate (<https://www.lfu.rlp.de>, last access: 9 May 2022) for gauges Müsch, Altenahr, Jünkerath, Kordel, Prüm 2, and Prümzurlay; Erftverband (<https://www.erftverband.de>, last access: 9 May 2022) for gauges Schönaus and Bliesheim; Wupperverband (<https://www.wupperverband.de>, last access: 9 May 2022) for gauges Hückeswagen and Opladen. The LAR-SIM hydrological simulations based on the PGW studies are available upon request from the Water administration of Rhineland-Palatinate. 970 The WRF model code can be obtained from <https://github.com/wrf-model/WRF/releases> (last access: 13 July 2022). ERA5-forcing data can be downloaded from the Copernicus Climate Change Service (C3S) Climate Date Store (<https://cds.climate.copernicus.eu/#/search?text=ERA5&type=dataset>, last access: 13 July 2022). LAERTES-EU, KIT-KLIWA, and the PGW simulation data can be requested from the authors. It is planned to provide parts via the German Climate Computing Center (DKRZ).

*Author contributions.* All KIT authors jointly designed the research questions of the study, continuously discussed the results, and wrote and 975 reviewed the text passages. BM and ACA were responsible for the analysis of historical precipitation events; FE worked on the statistical analysis of the LAERTES-EU data. UE, FS, and JD were responsible for the hydrological analyses (including collection and description of

the data). MF was responsible for the hydro-morphological part. MH and HF took care of the future climate projection; PL performed and analyzed the PGW simulations.

*Competing interests.* One of the coauthors (JGP) is a member of the editorial board of *Natural Hazards and Earth System Sciences*. The 980 peer-review process was guided by an independent editor, and the authors have also no other competing interests to declare.

*Acknowledgements.* This study is the result of an interdisciplinary collaboration at the Karlsruhe Institute of Technology (KIT), originating from a Forensic Disaster Analyses (FDA) on the flood of July 2021 conducted by the Center for Disaster Management and Risk Reduction Technology (CEDIM) in summer 2021. CEDIM is a cross-disciplinary research center in the field of disasters, risks, and security at KIT funded by the KIT and the research program “Changing Earth – Sustaining our Future” in the Helmholtz research field “Earth and Environment”. Several authors acknowledge partial funding from BMBF “ClimXtreme Module A” (01LP1901A), BMBF “RegIKlim-NUKLEUS” 985 (01LR2002B), BMBF “RegIKlim-ISAP” (01LR2007B) and DFG “Waves to Weather” TRR 165. Additionally, PL has been supported by the Helmholtz Association (Climate Initiative REKLIM grant) and JQ’s contribution was funded by the Young Investigator Group “Sub-seasonal Predictability: Understanding the Role of Diabatic Outflow” (SPREADOUT, grant VH-NG-1243). JGP thanks the AXA Research Fund for support (<https://axa-research.org/en/project/joaquim-pinto>, last access: 9 May 2022). The authors thank the Deutscher Wetterdienst (DWD) for providing the HYRAS, HYRAS-DE, KOSTRA, and RADOLAN data sets, and the German Climate Computation Center (DKRZ, Hamburg) for providing computing and storage resources under the projects 105 and 983. The authors thank the Water administration of Rhineland-Palatinate and Baden-Württemberg, the Erftverband, the Wupperverband, T. Roggenkamp from the University of Bonn, Germany, and the Global Runoff Data Center (GRDC), Koblenz (Germany), for providing valuable hydrological observational data and related evaluations. The authors thank the Water administration of Rhineland-Palatinate and HYDRON GmbH, Karlsruhe (Germany) for 990 carrying out all hydrological PGW simulations with LARSIM. Special thank goes to the *Kreisarchiv Ahrweiler* and Dieter Könnes for photo credits. We thank the reviewers for their valuable comments that helped to improve this study and the handling editor for guidance throughout the entire process. Finally, we thank the open-access publishing fund of KIT.

## References

Aalbers, E. E., van Meijgaard, E., Lenderink, G., de Vries, H., and van den Hurk, B. J. J. M.: The 2018 west-central European drought projected in a warmer climate: how much drier can it get?, *EGUphere*, 2022, 1–33, <https://doi.org/10.5194/egusphere-2022-954>, 2022.

Allen, M. R. and Ingram, W. J.: Constraints on future changes in climate and the hydrologic cycle, *Nature*, 419, 228–232, <https://doi.org/10.1038/nature01092>, 2002.

Amante, C. and Eakins, B.: ETOPO1 1 Arc-Minute Global Relief Model: Procedures, Data Sources and Analysis, National Geophysical Data Center, NESDIS, NOAA, US Dept, Commerce, Boulder, CO, USA, <https://doi.org/10.7289/V5C8276M>, 2008.

Annable, W., Lounder, V., and Watson, C.: Estimating channel-forming discharge in urban watercourses, *River Res. Appl.*, 27, 738–753, <https://doi.org/10.1002/rra.1391>, 2011.

Baldauf, M., Seifert, A., Förstner, J., Majewski, D., Raschendorfer, M., and Reinhardt, T.: Operational Convective-Scale Numerical Weather Prediction with the COSMO Model: Description and Sensitivities, *Mon. Weather Rev.*, 139, 3887–3905, <https://doi.org/10.1175/MWR-D-10-05013.1>, 2011.

Ban, N., Caillaud, C., Coppola, E., Pichelli, E., Sobolowski, S., Adinolfi, M., Ahrens, B., Alias, A., Anders, I., Bastin, S., et al.: The first multi-model ensemble of regional climate simulations at kilometer-scale resolution, part I: evaluation of precipitation, *Clim. Dynam.*, 57, 275–302, <https://doi.org/10.1007/s00382-021-05708-w>, 2021.

Bardossy, A., Seidel, J., Eisele, M., El Hachem, A., Kunstmänn, H., Chwala, C., Graf, M., Demuth, N., and Gerlach, N.: Verbesserung der Abschätzung von Gebietsniederschlägen mittels opportunistischer Niederschlagsmessungen am Beispiel des Ahr-Hochwassers im Juli 2021, *Hydrologie und Wasserbewirtschaftung*, 66, 208–214, 2022.

Beaty, C.: Debris flows, alluvial fans, and a revitalized catastrophism: *Zeitschrift für Geomorphologie*, supplement, v. 21, 1974.

Berg, P., Feldmann, H., and Panitz, H.-J.: Bias correction of high resolution regional climate model data, *J. Hydrol.*, 448, 80–92, <https://doi.org/10.1016/j.jhydrol.2012.04.026>, 2012.

Best, J., Ashmore, P., and Darby, S.: Beyond just floodwater, *Nat. Sustain.*, <https://doi.org/10.1038/s41893-022-00929-1>, 2022.

Bezak, N., Brilly, M., and Šraj, M.: Comparison between the peaks-over-threshold method and the annual maximum method for flood frequency analysis, *Hydrol. Sci. J.*, 59, 959–977, <https://doi.org/10.1080/02626667.2013.831174>, 2014.

BMDV: Verkehrsfreigabe der Teilstrecke Remagen-Ahrweiler, Bundesministerium für Digitales und Verkehr (BMDV), Berlin, Germany. Available: <https://www.bmvi.de/SharedDocs/DE/Artikel/K/ahrtal-bahn.html> (last access: 9 May 2022), 2021.

BMDV: Informationen zur Hochwasserkatastrophe, Bundesministerium für Digitales und Verkehr (BMDV), Berlin, Germany. Available: <https://www.bmvi.de/SharedDocs/DE/Artikel/K/unwetter.html> (last access: 9 May 2022), 2022.

Brabson, B. B. and Palutikof, J. P.: Tests of the Generalized Pareto Distribution for Predicting Extreme Wind Speeds, *J. Appl. Meteorol.*, 39, 1627–1640, [https://doi.org/10.1175/1520-0450\(2000\)039<1627:TGP>2.0.CO;2](https://doi.org/10.1175/1520-0450(2000)039<1627:TGP>2.0.CO;2), 2000.

Bung, D. B.: Extreme flooding in Western Germany: Some thoughts on hazards, return periods and risk, In: *Hydrolink 2021/4*. Madrid: International Association for Hydro-Environment Engineering and Research (IAHR), <https://www.iahr.org/library/hydrolink?hid=412>, last access: 8 August 2022, 2021.

Caldas-Alvarez, A., Augenstein, M., Ayzel, G., Barfus, K., Cherian, R., Dillenhardt, L., Fauer, F., Feldmann, H., Heistermann, M., Karwat, A., Kaspar, F., Kreibich, H., Lucio-Eceiza, E. E., Meredith, E. P., Mohr, S., Niermann, D., Pfahl, S., Ruff, F., Rust, H. W., Schoppa, L., Schwitalla, T., Steidl, S., Thielen, A. H., Tradowsky, J. S., Wulfmeyer, V., and Quaas, J.: Meteorological, impact and climate per-

pectives of the 29 June 2017 heavy precipitation event in the Berlin metropolitan area, *Nat. Hazards Earth Syst. Sci.*, 22, 3724–3724, 1035 https://doi.org/10.5194/nhess-22-3701-2022, 2022a.

Caldas-Alvarez, A., Feldmann, H., Lucio-Eceiza, E., and Pinto, J. G.: Scale-dependency of extreme precipitation processes in regional climate simulations of the greater Alpine region, *Weather Clim. Dyn. Disc.*, 2022, 1–37, https://doi.org/10.5194/wcd-2022-11, 2022b.

Cannon, D. J., Kirshbaum, D. J., and Gray, S. L.: Under what conditions does embedded convection enhance orographic precipitation?, *Q. J. R. Meteorol. Soc.*, 138, 391–406, https://doi.org/10.1002/qj.926, 2012.

1040 Chen, F., Janjić, Z., and Mitchell, K.: Impact of atmospheric surface-layer parameterizations in the new land-surface scheme of the NCEP mesoscale Eta model, *Boundary Layer Meteorol.*, 85, 391–421, https://doi.org/10.1023/A:1000531001463, 1997.

Collins, W. J., Bellouin, N., Doutriaux-Boucher, M., Gedney, N., Halloran, P., Hinton, T., Hughes, J., Jones, C. D., Joshi, M., Liddicoat, S., Martin, G., O'Connor, F., Rae, J., Senior, C., Sitch, S., Totterdell, I., Wiltshire, A., and Woodward, S.: Development and evaluation of an Earth-System model – HadGEM2, *Geosci. Model Dev.*, 4, 1051–1075, https://doi.org/10.5194/gmd-4-1051-2011, 2011.

1045 Copeland, R. R., Biedenharn, D. S., and Fischenich, J. C.: Channel-forming discharge, Tech. rep., Coastal and Hydraulics Laboratory (US), Engineer Research and Development Center (U.S.), 2000.

Crosato, A., Grisetti-Vázquez, A., Bregoli, F., and Franca, M.: Adaptation of river channels to a wetter or drier climate: insights from the Lower Pilcomayo River, South America, *J. Hydrol.*, p. 128254, https://doi.org/10.1016/j.jhydrol.2022.128254, 2022.

Dalcher, A. and Kalnay, E.: Error growth and predictability in operational ECMWF forecasts, *Tellus A*, 39, 474–491, 1050 https://doi.org/10.1111/j.1600-0870.1987.tb00322.x, 1987.

Dépret, T., Riquier, J., and Piégay, H.: Evolution of abandoned channels: Insights on controlling factors in a multi-pressure river system, *Geomorphology*, 294, 99–118, https://doi.org/10.1016/j.geomorph.2017.01.036, 2017.

Dewals, B., Erpicum, S., Pirotton, M., and Archambeau, P.: The July 2021 extreme floods in the Belgian part of the Meuse basin, *Hydrolink Magazine*, 4/2021, http://hdl.handle.net/2268/263750, 2021.

1055 Dietze, M. and Ozturk, U.: A flood of disaster response challenges, *Science*, 373, 1317–1318, https://doi.org/10.1126/science.abm0617, 2021.

Dietze, M., Bell, R., Ozturk, U., Cook, K. L., Andermann, C., Beer, A. R., Damm, B., Lucia, A., Fauer, F. S., Nissen, K. M., Sieg, T., and Thielen, A. H.: More than heavy rain turning into fast-flowing water — A landscape perspective on the 2021 Eifel floods, *Nat. Hazards Earth Syst. Sci.*, 22, 1845–1856, https://doi.org/10.5194/nhess-22-1845-2022, 2022.

1060 Doyle, M. W., Shields, D., Boyd, K. F., Skidmore, P. B., and Dominick, D.: Channel-forming discharge selection in river restoration design, *J. Hydraul. Eng.*, 133, 831–837, https://doi.org/10.1061/(ASCE)0733-9429(2007)133:7(831), 2007.

Eekhout, J. P. and de Vente, J.: Global impact of climate change on soil erosion and potential for adaptation through soil conservation, *Earth Sci. Rev.*, 226, 103 921, https://doi.org/10.1016/j.earscirev.2022.103921, 2022.

Ehmele, F., Kautz, L.-A., Feldmann, H., and Pinto, J. G.: Long-term variance of heavy precipitation across central Europe using a large 1065 ensemble of regional climate model simulations, *Earth Syst. Dynam.*, 11, 469–490, https://doi.org/10.5194/esd-11-469-2020, 2020.

Ehmele, F., Kautz, L.-A., Feldmann, H., He, Y., Kadlec, M., Kelemen, F. D., Lentink, H. S., Ludwig, P., Manful, D., and Pinto, J. G.: Adaptation and application of the large LAERTES-EU regional climate model ensemble for modeling hydrological extremes: a pilot study for the Rhine basin, *Nat. Hazards Earth Syst. Sci.*, 22, 677–692, https://doi.org/10.5194/nhess-22-677-2022, 2022.

Feldmann, H., Schädler, G., Panitz, H.-J., and Kottmeier, C.: Near future changes of extreme precipitation over complex terrain in Central 1070 Europe derived from high resolution RCM ensemble simulations, *Int. J. Climatol.*, 33, 1964–1977, https://doi.org/10.1002/joc.3564, 2013.

Feldmann, H., Pinto, J. G., Laube, N., Uhlig, M., Moemken, J., Pasternack, A., Früh, B., Pohlmann, H., and Kottmeier, C.: Skill and added value of the MiKlip regional decadal prediction system for temperature over Europe, *Tellus A: Dyn. Meteorol. Oceanogr.*, 71, 1618 678, <https://doi.org/10.1080/16000870.2019.1618678>, 2019.

Frei, C., Davies, H. C., Gurtz, J., and Schär, C.: Climate dynamics and extreme precipitation and flood events in Central Europe, *Integrated Assessment*, 1, 281–300, <https://doi.org/10.1023/A:1018983226334>, 2000.

Früh, B., Feldmann, H., Panitz, H.-J., Schädler, G., Jacob, . D., Lorenz, P., and Keuler, K.: Determination of Precipitation Return Values in Complex Terrain and Their Evaluation, *J. Climate*, 23, 2257–2274, <https://doi.org/10.1175/2009JCLI2685.1>, 2010.

Fuhrer, O. and Schär, C.: Embedded Cellular Convection in Moist Flow past Topography, *J. Atmos. Sci.*, 62, 2810 – 2828, <https://doi.org/10.1175/JAS3512.1>, 2005.

Giorgetta, M. A., Jungclaus, J., Reick, C. H., Legutke, S., Bader, J., Böttinger, M., Brovkin, V., Crueger, T., Esch, M., Fieg, K., Glushak, K., Gayler, V., Haak, H., Hollweg, H.-D., Ilyina, T., Kinne, S., Kornblueh, L., Matei, D., Mauritsen, T., Mikolajewicz, U., Müller, W., Notz, D., Pithan, F., Raddatz, T., Rast, S., Redler, R., Roeckner, E., Schmidt, H., Schnur, R., Segschneider, J., Six, K. D., Stockhause, M., Timmreck, C., Wegner, J., Widmann, H., Wieners, K.-H., Claussen, M., Marotzke, J., and Stevens, B.: Climate and carbon cycle changes from 1850 to 2100 in MPI-ESM simulations for the Coupled Model Intercomparison Project phase 5, *J. Adv. Model. Earth Sy.*, 5, 572–597, <https://doi.org/10.1002/jame.20038>, 2013.

Grieser, J., Staeger, T., and Schönwiese, C.-D.: Estimates and uncertainties of return periods of extreme daily precipitation in Germany, *Meteorol. Z.*, 16, 553–564, <https://doi.org/10.1127/0941-2948/2007/0235>, 2007.

Gumbel, E. J.: The return period of flood flows, *The annals of mathematical statistics*, 12, 163–190, 1941.

Hackenbruch, J., Schädler, G., and Schipper, J.: Added value of high-resolution regional climate simulations for regional impact studies, *Meteorol. Z.*, 25, 291–304, <https://doi.org/10.1127/metz/2016/0701>, 2016.

Harrison, S., Mighall, T., Stainforth, D. A., Allen, P., Macklin, M., Anderson, E., Knight, J., Mauquoy, D., Passmore, D., Rea, B., et al.: Uncertainty in geomorphological responses to climate change, *Clim. Change*, 156, 69–86, <https://doi.org/10.1007/s10584-019-02520-8>, 2019.

Haylock, M., Hofstra, N., Tank, A. K., Klok, E., Jones, P., and New, M.: A European daily high-resolution gridded data set of surface temperature and precipitation for 1950–2006, *J. Geophys. Res.*, 113, <https://doi.org/10.1029/2008JD010201>, 2008.

Heggen, R. J.: Normalized antecedent precipitation index, *J. Hydrol. Eng.*, 6, 377–381, [https://doi.org/10.1061/\(ASCE\)1084-0699\(2001\)6:5\(377\)](https://doi.org/10.1061/(ASCE)1084-0699(2001)6:5(377)), 2001.

Henrichs, Y.: personal communication in the context of flood hazard maps, 2022.

Hersbach, H., Bell, B., Berrisford, P., Hirahara, S., Horányi, A., Muñoz-Sabater, J., Nicolas, J., Peubey, C., Radu, R., Schepers, D., Simmons, A., Soci, C., Abdalla, S., Abellán, X., Balsamo, G., Bechtold, P., Biavati, G., Bidlot, J., Bonavita, M., De Chiara, G., Dahlgren, P., Dee, D., Diamantakis, M., Dragani, R., Flemming, J., Forbes, R., Fuentes, M., Geer, A., Haimberger, L., Healy, S., Hogan, R. J., Hólm, E., Janisková, M., Keeley, S., Laloyaux, P., Lopez, P., Lupu, C., Radnoti, G., de Rosnay, P., Rozum, I., Vamborg, F., Villaume, S., and Thépaut, J.-N.: The ERA5 global reanalysis, *Q. J. R. Meteorol. Soc.*, 146, 1999–2049, <https://doi.org/10.1002/qj.3803>, 2020.

Iacono, M. J., Delamere, J. S., Mlawer, E. J., Shephard, M. W., Clough, S. A., and Collins, W. D.: Radiative forcing by long-lived greenhouse gases: Calculations with the AER radiative transfer models, *J. Geophys. Res. Atmos.*, 113, <https://doi.org/10.1029/2008JD009944>, 2008.

IPCC: Contribution of working group I to the sixth assessment report of the intergovernmental panel on climate change, in: *Climate change 2021: the physical science basis.*, edited by Masson-Delmotte, V., Zhai, P., Pirani, A., Connors, S., Péan, C., Berger, S., Caud, N., Chen,

Y., Goldfarb, L., Gomis, M., Huang, M., Leitzell, K., Lonnoy, E., Matthews, J., Maycock, T., Waterfield, T., Yelekçi, O., Yu, R., and Zhou, B., Cambridge University Press, Cambridge, UK and New York, NY, USA (in press), <https://doi.org/10.1017/9781009157896>, 2021a.

1110 IPCC: Annex II: Models, in: Climate change 2021: the physical science basis., edited by Masson-Delmotte, V., Zhai, P., Pirani, A., Connors, S., Péan, C., Berger, S., Caud, N., Chen, Y., Goldfarb, L., Gomis, M., Huang, M., Leitzell, K., Lonnoy, E., Matthews, J., Maycock, T., Waterfield, T., Yelekçi, O., Yu, R., and Zhou, B., Cambridge University Press, Cambridge, UK and New York, NY, USA (in press), <https://doi.org/10.1017/9781009157896.016>, 2021b.

IPCC: Contribution of Working Group III to the Sixth Assessment Report of the Intergovernmental Panel on Climate Change, in: Climate 1115 Change 2022: Mitigation of Climate Change., edited by Shukla, P., Skea, J., Slade, R., Khoardajie, A. A., van Diemen, R., McCollum, D., Pathak, M., Some, S., Vyas, P., Fradera, R., Belkacemi, M., Hasija, A., Lisboa, G., Luz, S., and Malley, J., Cambridge University Press, Cambridge, UK and New York, NY, USA, <https://doi.org/10.1017/9781009157926>, 2022.

Janjić, Z. I.: The Step-Mountain Eta Coordinate Model: Further Developments of the Convection, Viscous Sublayer, and Turbulence Closure Schemes, *Mon. Weather Rev.*, 122, 927–945, [https://doi.org/10.1175/1520-0493\(1994\)122<0927:TSMECM>2.0.CO;2](https://doi.org/10.1175/1520-0493(1994)122<0927:TSMECM>2.0.CO;2), 1994.

1120 Junghänel, T., Ertel, H., and Deutschländer, T.: KOSTRA-DWD-2010R. Bericht zur Revision der koordinierten Starkregenregionalisierung und-auswertung des Deutschen Wetterdienstes in der Version 2010, Deutscher Wetterdienst, [https://www.dwd.de/DE/leistungen/kostra\\_dwd\\_rasterwerte/download/bericht\\_revision\\_kostra\\_dwd\\_2010](https://www.dwd.de/DE/leistungen/kostra_dwd_rasterwerte/download/bericht_revision_kostra_dwd_2010) (last access: 4 March 2022), 2017.

Junghänel, T., Bissolli, P., Daßler, J., Fleckenstein, R., Imbery, F., Janssen, W., Kaspar, F., Lengfeld, K., Leppe, T., Rauthe, M., Rauthe-Schöch, A., Rocek, M., Walawender, E., and Weigl, E.: Hydro-klimatologische 1125 Einordnung der Stark- und Dauerniederschläge in Teilen Deutschlands im Zusammenhang mit dem Tiefdruckgebiet „Bernd“ vom 12. bis 19. Juli 2021, Deutscher Wetterdienst (DWD), Offenbach, Germany. Available: [https://www.dwd.de/DE/leistungen/besondereereignisse/niederschlag/20210721\\_bericht\\_starkniederschlaege\\_tief\\_bernd.html](https://www.dwd.de/DE/leistungen/besondereereignisse/niederschlag/20210721_bericht_starkniederschlaege_tief_bernd.html) (last access: 24 January 2022), 2021.

Kautz, L.-A., Martius, O., Pfahl, S., Pinto, J. G., Ramos, A. M., Sousa, P. M., and Woollings, T.: Atmospheric blocking and weather extremes 1130 over the Euro-Atlantic sector—a review, *Weather Clim. Dyn.*, 3, 305–336, <https://doi.org/10.5194/wcd-2021-56>, 2022.

Kelemen, F. D., Ludwig, P., Reyers, M., Ulbrich, S., and Pinto, J. G.: Evaluation of moisture sources for the Central European summer flood of May/June 2013 based on regional climate model simulations, *Tellus A: Dyn. Meteorol. Oceanogr.*, 68, 29 288, <https://doi.org/10.3402/tellusa.v68.29288>, 2016.

Kern, K.: Grundlagen naturnaher Gewässergestaltung: Geomorphologische Entwicklung von Fließgewässern, Springer-Verlag, 2013.

1135 Kohler, M. A. and Linsley, R. K.: Predicting the runoff from storm rainfall, vol. 30, US Department of Commerce, Weather Bureau, 1951.

Kreienkamp, F., Philip, S. Y., Tradowsky, J. S., Kew, S. F., Lorenz, P., Arrighi, J., Belleflamme, A., Bettmann, T., Caluwaerts, S., Chan, S. C., Ciavarella, A., Cruz, L. D., de Vries, H., Demuth, N., Ferrone, A., Fischer, E. M., Fowler, H. J., Goergen, K., Heinrich, D., Henrichs, Y., Lenderink, G., Kaspar, F., Nilson, E., Otto, F. E. L., Ragone, F., Seneviratne, S. I., Singh, R. K., Skålevåg, A., Termonia, P., Thalheimer, L., van Aalst, M., den Bergh, J. V., de Vyver, H. V., Stéphane Vannitsem and, G. J. v. O., Schaebybroeck, B. V., Vautard, R., Vonk, D., and 1140 Wanders, N.: Rapid attribution of heavy rainfall events leading to the severe flooding in Western Europe during July 2021, World Weather Attribution (WWA). Available: <https://www.worldweatherattribution.org/heavy-rainfall-which-led-to-severe-flooding-in-western-europe-made-more-likely-by-climate-change/> (last access: 3 December 2021), 2021.

Kunz, M., Mühr, B., Kunz-Plapp, T., Daniell, J., Khazai, B., Wenzel, F., Vannieuwenhuyse, M., Comes, T., Elmer, F., Schröter, K., et al.: Investigation of superstorm Sandy 2012 in a multi-disciplinary approach, *Nat. Hazards Earth Syst. Sci.*, 13, 2579–2598, 1145 <https://doi.org/10.5194/nhess-13-2579-2013>, 2013.

Lackmann, G. M.: The South-Central U.S. Flood of May 2010: Present and Future, *Journal of Climate*, 26, 4688 – 4709, <https://doi.org/10.1175/JCLI-D-12-00392.1>, 2013.

Lane, S., Tayefi, V., Reid, S., Yu, D., and Hardy, R.: Interactions between sediment delivery, channel change, climate change and flood risk in a temperate upland environment, *Earth Surf. Process. Landf.*, 32, 429–446, <https://doi.org/10.1002/esp.1404>, 2007.

1150 Le Coz, J., Hauet, A., Pierrefeu, G., Dramaïs, G., and Camenon, B.: Performance of image-based velocimetry (LSPIV) applied to flash-flood discharge measurements in Mediterranean rivers, *J. Hydrol.*, 394, 42–52, <https://doi.org/10.1016/j.jhydrol.2010.05.049>, 2010.

Lenderink, G., Barbero, R., Loriaux, J. M., and Fowler, H. J.: Super-Clausius–Clapeyron Scaling of Extreme Hourly Convective Precipitation and Its Relation to Large-Scale Atmospheric Conditions, *Journal of Climate*, 30, 6037 – 6052, <https://doi.org/10.1175/JCLI-D-16-0808.1>, 2017.

1155 Lenderink, G., de Vries, H., Fowler, H. J., Barbero, R., van Ulft, B., and van Meijgaard, E.: Scaling and responses of extreme hourly precipitation in three climate experiments with a convection-permitting model, *Philosophical Transactions of the Royal Society A: Mathematical, Physical and Engineering Sciences*, 379, 20190544, <https://doi.org/10.1098/rsta.2019.0544>, 2021.

Lorenz, E. N.: Atmospheric predictability experiments with a large numerical model, *Tellus A*, 34, 505–513, <https://doi.org/10.3402/tellusa.v34i6.10836>, 1982.

1160 LUBW: Festlegung des Bemessungshochwassers für Anlagen des technischen Hochwasserschutzes, Tech. rep., Landesanstalt für Umweltschutz Baden-Württemberg (LUBW), 2005.

Lucía, A., Schwientek, M., Eberle, J., and Zarfl, C.: Planform changes and large wood dynamics in two torrents during a severe flash flood in Braunsbach, Germany 2016, *Sci. Total Environ.*, 640, 315–326, <https://doi.org/10.1016/j.scitotenv.2018.05.186>, 2018.

Ludwig, K. and Bremicker, M.: The Water Balance Model LARSIM - Design, Content and Applications, vol. 22 of *Freiburger Schriften zur Hydrologie*, Institut für Hydrologie, Uni Freiburg i. Br., <https://www.larsim.info/en/>, 2006.

1165 Madsen, H., Rasmussen, P. F., and Rosbjerg, D.: Comparison of annual maximum series and partial duration series methods for modeling extreme hydrologic events: 1. At-site modeling, *Water Resour. Res.*, 33, 747–757, <https://doi.org/10.1029/96WR03848>, 1997.

Magilligan, F. J., Phillips, J. D., James, L. A., and Gomez, B.: Geomorphic and sedimentological controls on the effectiveness of an extreme flood, *J. Geol.*, 106, 87–96, <https://doi.org/10.1086/516009>, 1998.

1170 Maher, N., Milinski, S., and Ludwig, R.: Large ensemble climate model simulations: introduction, overview, and future prospects for utilising multiple types of large ensemble, *Earth System Dynamics*, 12, 401–418, <https://doi.org/10.5194/esd-12-401-2021>, 2021.

Malitz, G. and Ertel, H.: KOSTRA DWD 2010: Starkniederschlagsröhnen für Deutschland (Bezugszeitraum 1951 bis 2010); Abschlussbericht, Deutscher Wetterdienst, [https://www.dwd.de/DE/leistungen/kostra\\_dwd\\_rasterwerte/download/bericht\\_kostra\\_dwd\\_2010\\_pdf.html](https://www.dwd.de/DE/leistungen/kostra_dwd_rasterwerte/download/bericht_kostra_dwd_2010_pdf.html) (last access: 4 March 2022), 2015.

1175 Marotzke, J., Müller, W. A., Vamborg, F. S., Becker, P., Cubasch, U., Feldmann, H., Kaspar, F., Kottmeier, C., Marini, C., Polkova, I., Prömmel, K., Rust, H. W., Stammer, D., Ulbrich, U., Kadow, C., Köhl, A., Kröger, J., Kruschke, T., Pinto, J. G., Pohlmann, H., Reyers, M., Schröder, M., Sienz, F., Timmreck, C., and Ziese, M.: MiKlip: a national research project on decadal climate prediction, *Bull. Am. Meteorol. Soc.*, 97, 2379–2394, <https://doi.org/10.1175/BAMS-D-15-00184.1>, 2016.

Marx, S.: Die im Gebiet der DDR aufgetretenen extrem hohen Tagessummen des Niederschlages (1907 bis 1978) mit Angaben über die Ausmaße des starken Dauerregens vom 7./8. August 1978, *Zeitschrift für Meteorologie*, 30, 318–328, 1980.

1180 Meinshausen, M., Smith, S., Calvin, K., and et al.: he RCP greenhouse gas concentrations and their extensions from 1765 to 2300, *Clim. Change*, pp. 219–231, <https://doi.org/10.1007/s10584-011-0156-z>, 2011.

Merz, B., Elmer, F., Kunz, M., Mühr, B., Schröter, K., and Uhlemann-Elmer, S.: The extreme flood in June 2013 in Germany, *Houille Blanche*, 100, 5–10, <https://doi.org/10.1051/lhb/2014001>, 2014.

1185 Messmer, M., Gómez-Navarro, J. J., and Raible, C. C.: Climatology of Vb cyclones, physical mechanisms and their impact on extreme precipitation over Central Europe, *Earth System Dynamics*, 6, 541–553, <https://doi.org/10.5194/esd-6-541-2015>, 2015.

MeteoLux: Hochwasserereignis Juli 2021, Météo au Luxembourg (MeteoLux), l'Administration de la navigation aérienne, Luxembourg. Available: <https://www.meteolux.lu/de/aktuelles/rückblick-auf-den-ergiebigen-dauerregen-vom-14-und-15-juli-2021> (last access: 24 January 2022), 2021.

1190 Michaelis, A. C., Willison, J., Lackmann, G. M., and Robinson, W. A.: Changes in winter North Atlantic extratropical cyclones in high-resolution regional pseudo-global warming simulations, *J. Climate*, 30, 6905–6925, <https://doi.org/10.1175/JCLI-D-16-0697.1>, 2017.

Mohr, S., Ehret, U., Kunz, M., Ludwig, P., Caldas-Alvarez, A., Daniell, J. E., Ehmele, F., Feldmann, H., Franca, M. J., Gattke, C., Hundhausen, M., Knippertz, P., Küpfer, K., Mühr, B., Pinto, J. G., Quinting, J., Schäfer, A. M., Scheibel, M., Seidel, F., and Wisotzky, C.: A multi-disciplinary analysis of the exceptional flood event of July 2021 in central Europe. Part 1: Event description and analysis, *Nat. Hazards Earth Syst. Sci. Disc.*, <https://doi.org/10.5194/nhess-2022-137>, 2022.

1195 Mudelsee, M., Börngen, M., Tetzlaff, G., and Grünwald, U.: Extreme floods in central Europe over the past 500 years: Role of cyclone pathway “Zugstrasse Vb”, *J. Geophys. Res. Atmos.*, 109, <https://doi.org/10.1029/2004JD005034>, 2004.

Munich Re: Hurricanes, cold waves, tornadoes: Weather disasters in USA dominate natural disaster losses in 2021 – Europe: Extreme flash floods with record losses, Munich Re, Media relations on January 10, 2022: Natural disaster losses 2021, Munich Germany. Available: <https://www.munichre.com/en/company/media-relations/media-information-and-corporate-news/media-information/2022/natural-disaster-losses-2021.html> (last access: 9 May 2022), 2022.

1200 Nones, M., Gerstgraser, C., and Wharton, G.: Consideration of hydromorphology and sediment in the implementation of the EU water framework and floods directives: a comparative analysis of selected EU member states, *Water Environ. J.*, 31, 324–329, <https://doi.org/10.1111/wej.12247>, 2017.

1205 Otto, F. E.: Attribution of weather and climate events, *Ann. Rev. Env. Resour.*, 42, 627–646, <https://doi.org/10.1146/annurevviron-102016-060847>, 2017.

O’Gorman, P. A.: Precipitation extremes under climate change, *Current climate change reports*, 1, 49–59, <https://doi.org/10.1007/s40641-015-0009-3>, 2015.

Pall, P., Allen, M., and Stone, D. A.: Testing the Clausius–Clapeyron constraint on changes in extreme precipitation under CO<sub>2</sub> warming, *Climate Dynamics*, 28, 351–363, <https://doi.org/10.1007/s00382-006-0180-2>, 2007.

1210 Pender, D., Patidar, S., Hassan, K., and Haynes, H.: Method for incorporating morphological sensitivity into flood inundation modeling, *J. Hydraul. Eng.*, 142, 04016008, [https://doi.org/10.1061/\(ASCE\)HY.1943-7900.0001127](https://doi.org/10.1061/(ASCE)HY.1943-7900.0001127), 2016.

Piper, D., Kunz, M., Ehmele, F., Mohr, S., Mühr, B., Kron, A., and Daniell, J.: Exceptional sequence of severe thunderstorms and related flash floods in May and June 2016 in Germany. Part I: Meteorological background, *Nat. Hazards Earth Syst. Sci.*, 16, 2835–2850, <https://doi.org/10.5194/nhess-16-2835-2016>, 2016.

1215 Prein, A. F., Langhans, W., Fosser, G., Ferrone, A., Ban, N., Goergen, K., Keller, M., Tölle, M., Gutjahr, O., Feser, F., Brisson, E., Kollet, S., Schmidli, J., van Lipzig, N. P. M., and Leung, R.: A review on regional convection-permitting climate modeling: Demonstrations, prospects, and challenges, *Rev. Geophys.*, 53, 323–361, <https://doi.org/10.1002/2014RG000475>, 2015.

Prodhomme, C., Doblas-Reyes, F. J., Bellprat, O., and Dutra, E.: Impact of land-surface initialization on sub-seasonal to seasonal forecasts over Europe, *Clim. Dynam.*, 47, 919–935, <https://doi.org/10.1007/s00382-015-2879-4>, 2016.

Radice, A., Longoni, L., Papini, M., Brambilla, D., and Ivanov, V.: Generation of a design flood-event scenario for a mountain river with intense sediment transport, *Water*, 8, 597, <https://doi.org/10.3390/w8120597>, 2016.

Rauthe, M., Steiner, H., Riediger, U., A., M., and Gratzki, A.: A Central European precipitation climatology – Part I: Generation and validation of a high-resolution gridded daily data set (HYRAS), *Meteorol. Z.*, 22, 235–256, <https://doi.org/10.1127/0941-2948/2013/0436>, 2013.

1225 RedaktionsNetzwerk Deutschland: Ein Jahr nach der Flutkatastrophe: So geht es den Menschen im Ahrtal, RedaktionsNetzwerk Deutschland, Hanover, Germany, 20 June 2022. Available: <https://www.rnd.de/panorama/ahrtal-so-geht-es-den-menschen-nach-der-flutkatastrophe-LEXREN3YXKOQEAHK2FK4POQULRM.html> (last access: 1 February 2023), 2022.

1230 Regenauer, J., Böhm, M., and Gerlinger, K.: Nachrechnung des Hochwassers an der Ahr am 14./15. Juli 2021 mit dem LARSIM-Wasserhaushaltsmodell für Rheinland-Pfalz, Report, HYDRON - Ingenieurgesellschaft für Umwelt und Wasserwirtschaft mbH, Karlsruhe, 2022.

Roggenkamp, T. and Herget, J.: Reconstructing peak discharges of historic floods of the River Ahr, Germany, in: *Erdkunde* 68, pp. 49–59, 2014a.

1235 Roggenkamp, T. and Herget, J.: Historische Hochwasser der Ahr – Die Rekonstruktion von Scheitelabflüssen ausgewählter Ahr-Hochwasser, in: *Heimatjahrbuch Kreis Ahrweiler 2015*, edited by Ahrweiler, L., pp. 150–154, 2014b.

Roggenkamp, T. and Herget, J.: Hochwasser der Ahr im Juli 2021 – Abflusseinschätzung und Einordnung, Hydrologie und Wasserbewirtschaftung (HyWa), 66, 40–49, 2022.

Schädler, G., Panitz, H.-J., Christner, E., Feldmann, H., Karremann, M., and Laube, N.: Regional Climate Simulations with COSMO-CLM: 1240 Ensembles, Very High Resolution and Paleoclimate, in: *High Performance Computing in Science and Engineering '17*, edited by Nagel, W. E., Kröner, D. H., and Resch, M. M., pp. 411–429, Springer International Publishing, [https://doi.org/10.1007/978-3-319-68394-2\\_24](https://doi.org/10.1007/978-3-319-68394-2_24), 2018.

Schäfer, A., Mühr, B., Daniell, J. E., Ehret, U., Ehmele, F., Küpfer, K., Brand, J., Wisotzky, C., Skapski, J., Rentz, L., Mohr, S., and Kunz, M.: CEDIM Forensic Disaster Analysis (FDA) Group „Hochwasser Mitteleuropa, Juni 2021 (Deutschland)“ Bericht Nr. 1245 1 „Nordrhein-Westfalen & Rheinland-Pfalz“, Center for Disaster Management and Risk Reduction Technology, Karlsruhe, Germany, <https://doi.org/10.5445/IR/1000135730>, 2021.

Schär, C., Frei, C., Lüthi, D., and Davies, H. C.: Surrogate climate-change scenarios for regional climate models, *Geophys. Res. Lett.*, 23, 669–672, <https://doi.org/10.1029/96GL00265>, 1996.

Schröter, K., Kunz, M., Elmer, F., Mühr, B., and Merz, B.: What made the June 2013 flood in Germany an exceptional event? A hydro-1250 meteorological evaluation, *Hydrol. Earth Syst. Sci.*, 19, 309–327, <https://doi.org/10.5194/hess-19-309-2015>, 2015.

Seel, K. A.: Die Ahr und ihre Hochwässer in alten Quellen, *Heimatjahrbuch des Kreises Ahrweiler*, 40, 91–102, 1983.

Seminara, G.: Fluvial sedimentary patterns, *Annu. Rev. Fluid Mech.*, 42, 43–66, <https://doi.org/10.1146/annurev-fluid-121108-145612>, 2010.

Shepherd, T. G.: A common framework for approaches to extreme event attribution, *Current Climate Change Reports*, 2, 28–38, <https://doi.org/10.1007/s40641-016-0033-y>, 2016.

1255 Shepherd, T. G.: Storyline approach to the construction of regional climate change information, *P. Roy. Soc. A - Math. Phy.*, 475, 20190 013, <https://doi.org/10.1098/rspa.2019.0013>, 2019.

Shepherd, T. G., Boyd, E., Calel, R. A., Chapman, S. C., Dessai, S., Dima-West, I. M., Fowler, H. J., James, R., Maraun, D., Martius, O., et al.: Storylines: an alternative approach to representing uncertainty in physical aspects of climate change, *Clim. Dynam.*, 151, 555–571, <https://doi.org/10.1007/s10584-018-2317-9>, 2018.

1260 Sillmann, J., Shepherd, T. G., van den Hurk, B., Hazeleger, W., Martius, O., Slingo, J., and Zscheischler, J.: Event-Based Storylines to Address Climate Risk, *Earth's Future*, 9, e2020EF001 783, <https://doi.org/10.1029/2020EF001783>, 2021.

Skamarock, W. C., Klemp, J. B., Dudhia, J., Gill, D. O., Liu, Z., Berner, J., Wang, W., Powers, J. G., Duda, M. G., Barker, D. M., and Huang, X.-Y.: A description of the advanced research WRF model version 4, National Center for Atmospheric Research: Boulder, CO, USA, p. 145, 2019.

1265 Sørland, S. L., Brogli, R., Pothapakula, P. K., Russo, E., Van de Walle, J., Ahrens, B., Anders, I., Bucchignani, E., Davin, E. L., Demory, M.-E., Dosio, A., Feldmann, H., Früh, B., Geyer, B., Keuler, K., Lee, D., Li, D., van Lipzig, N. P. M., Min, S.-K., Panitz, H.-J., Rockel, B., Schär, C., Steger, C., and Thiery, W.: COSMO-CLM regional climate simulations in the Coordinated Regional Climate Downscaling Experiment (CORDEX) framework: A review, *Geosci. Model Dev.*, 14, 5125–5154, <https://doi.org/10.5194/gmd-2020-443>, 2021.

1270 Stocker, T.: Climate change 2013: the physical science basis: Working Group I contribution to the Fifth assessment report of the Intergovernmental Panel on Climate Change, Cambridge university press, 2014.

Stott, P. A., Stone, D. A., and Allen, M. R.: Human contribution to the European heatwave of 2003, *Nature*, 432, 610–614, <https://doi.org/10.1038/nature03089>, 2004.

Stott, P. A., Christidis, N., Otto, F. E., Sun, Y., Vanderlinden, J.-P., van Oldenborgh, G. J., Vautard, R., von Storch, H., Walton, P., Yiou, P., et al.: Attribution of extreme weather and climate-related events, *Wiley Interdisciplinary Reviews: Climate Change*, 7, 23–41, <https://doi.org/10.1002/wcc.380>, 2016.

1275 Stucki, P., Rickli, R., Brönnimann, S., Martius, O., Wanner, H., Grebner, D., and Luterbacher, J.: Weather patterns and hydro-climatological precursors of extreme floods in Switzerland since 1868, *Meteorol. Z.*, 21, 531–550, <https://doi.org/10.1127/0941-2948/2012/368>, 2012.

Szymczak, S., Backendorf, F., Bott, F., Fricke, K., Junghänel, T., and Walawender, E.: Impacts of Heavy and Persistent Precipitation on Railroad Infrastructure in July 2021: A Case Study from the Ahr Valley, Rhineland-Palatinate, Germany, *Atmosphere*, 13, <https://doi.org/10.3390/atmos13071118>, 2022.

1280 Sánchez-Benítez, A., Goessling, H., Pithan, F., Semmler, T., and Jung, T.: The July 2019 European Heat Wave in a Warmer Climate: Storyline Scenarios with a Coupled Model Using Spectral Nudging, *Journal of Climate*, 35, 2373 – 2390, <https://doi.org/10.1175/JCLI-D-21-0573.1>, 2022.

Taylor, K. E., Stouffer, R. J., and Meehl, G. A.: An Overview of CMIP5 and the Experiment Design, *Bull. Am. Meteorol. Soc.*, 93, 485–498, <https://doi.org/10.1175/BAMS-D-11-00094.1>, 2012.

1285 Teichmann, C., Bülow, K., Otto, J., Pfeifer, S., Rechid, D., Sieck, K., and Jacob, D.: Avoiding extremes: benefits of staying below +1.5 °C compared to +2.0 °C and +3.0 °C global warming, *Atmosphere*, 9, 115, <https://doi.org/10.3390/atmos9040115>, 2018.

Thompson, G., Field, P. R., Rasmussen, R. M., and Hall, W. D.: Explicit Forecasts of Winter Precipitation Using an Improved Bulk Microphysics Scheme. Part II: Implementation of a New Snow Parameterization, *Mon. Weather Rev.*, 136, 5095–5115, <https://doi.org/10.1175/2008MWR2387.1>, 2008.

1290 Tradowsky, J. S., Philip, S. Y., Kreienkamp, F., Kew, S. F., Lorenz, P., Arrighi, J., Belleflamme, A., Bettmann, T., Caluwaerts, S., Chan, S. C., Ciavarella, A., De Cruz, L., de Vries, H., Demuth, N., Ferrone, A., Fischer, E. M., Fowler, H. J., Goergen, K., Heinrich, D., Henrichs, Y., Lenderink, G., Kaspar, F., Nilson, E., Otto, F. E. L., Ragone, F., Seneviratne, S. I., Singh, R. K., Skålevåg, A., Termonia, P., Thalheimer, L., van Aalst, M., Van den Bergh, J., Van de Vyver, H., Vannitsem, S., van Oldenborgh, G. J., Van Schaeybroeck, B., Vautard, R., Vonk,

1295 D., and Wanders, N.: Attribution of heavy rainfall events leading to the severe flooding in Western Europe during July 2021, *Clim. Change* in revision., 2022.

Trenberth, K. E., Dai, A., Rasmussen, R. M., and Parsons, D. B.: The Changing Character of Precipitation, *Bull. Am. Meteorol. Soc.*, 84, 1205 – 1218, <https://doi.org/10.1175/BAMS-84-9-1205>, 2003.

Trenberth, K. E., Fasullo, J. T., and Shepherd, T. G.: Attribution of climate extreme events, *Nat. Clim. Change*, 5, 725–730, 1300 <https://doi.org/10.1038/nclimate2657>, 2015.

Trier, S. B., Parsons, D. B., and Clark, J. H. E.: Environment and Evolution of a Cold-Frontal Mesoscale Convective System, *Mon. Weather Rev.*, 119, 2429 – 2455, [https://doi.org/10.1175/1520-0493\(1991\)119<2429:EAEOAC>2.0.CO;2](https://doi.org/10.1175/1520-0493(1991)119<2429:EAEOAC>2.0.CO;2), 1991.

Ulbrich, U., Brücher, T., Fink, A. H., Leckebusch, G. C., Krüger, A., and Pinto, J. G.: The central European floods of August 2002: Part 1–Rainfall periods and flood development, *Weather*, 58, 371–377, <https://doi.org/10.1256/wea.61.03A>, 2003.

1305 van Bebber, W. J.: Die Zugstrassen der barometrischen Minima nach den Bahnennkarten der deutschen Seewarte für den Zeitraum 1875–1890, *Meteorol. Z.*, 8, 361–266, 1891.

van Garderen, L., Feser, F., and Shepherd, T. G.: A methodology for attributing the role of climate change in extreme events: a global spectrally nudged storyline, *Natural Hazards and Earth System Sciences*, 21, 171–186, <https://doi.org/10.5194/nhess-21-171-2021>, 2021.

Vergara-Temprado, J., Ban, N., and Schär, C.: Extreme Sub-Hourly Precipitation Intensities Scale Close to the Clausius-Clapeyron Rate Over 1310 Europe, *Geophysical Research Letters*, 48, e2020GL089 506, <https://doi.org/10.1029/2020GL089506>, 2021.

Viessman, W., Lewis, G. L., Knapp, J. W., and Harbaugh, T. E.: *Introduction to Hydrology*, 612 pp., Prentice Hall, New York, USA, 5 edn., 2002.

Volodioire, A., Sanchez-Gomez, E., Salas y Mélia, D., Decharme, B., Cassou, C., Sénési, S., Valcke, S., Beau, I., Alias, A., Chevallier, M., Déqué, M., Deshayes, J., Douville, H., Fernandez, E., Madec, G., Maisonnave, E., Moine, M.-P., Planton, S., Saint-Martin, D., Szopa, S., 1315 Tyteca, S., Alkama, R., Belamari, S., Braun, A., Coquart, L., and F., C.: The CNRM-CM5.1 global climate model: description and basic evaluation, *Clim. Dynam.*, 40, 2091–2121, <https://doi.org/10.1007/s00382-011-1259-y>, 2013.

von Storch, H., Langenberg, H., and Feser, F.: A Spectral Nudging Technique for Dynamical Downscaling Purposes, *Mon. Weather Rev.*, 128, 3664 – 3673, [https://doi.org/10.1175/1520-0493\(2000\)128<3664:ASNTFD>2.0.CO;2](https://doi.org/10.1175/1520-0493(2000)128<3664:ASNTFD>2.0.CO;2), 2000.

Vorogushyn, S., Apel, H., Kemter, M., and Thielen, A.: Analyse der Hochwassergefährdung im Ahrtal unter Berücksichtigung historischer 1320 Hochwasser, *Hydrologie & Wasserbewirtschaftung*, 66, 244–254, [https://doi.org/10.5675/HyWa\\_2022.5\\_2](https://doi.org/10.5675/HyWa_2022.5_2), 2022.

Weckwerth, T. M. and Parsons, D. B.: A Review of Convection Initiation and Motivation for IHOP\_2002, *Mon. Weather Rev.*, 134, 5 – 22, <https://doi.org/10.1175/MWR3067.1>, 2006.

Weigl, E. and Winterrath, T.: Radargestützte Niederschlagsanalyse und –vorhersage (RADOLAN, RADVOR-OP), *Promet*, 35, 78–86, 2009.

Wilhelm, J., Mohr, S., Punge, H. J., Mühr, B., Schmidberger, M., Daniell, J. E., Bedka, K. M., and Kunz, M.: Severe thunderstorms with 1325 large hail across Germany in June 2019, *Weather*, 76, 228–237, <https://doi.org/10.1002/wea.3886>, 2021.

Wilks, D. S.: *Statistical methods in the atmospheric sciences*, International geophysics series ; 91, Elsevier Acad. Press, 2. ed. edn., 2006.

Winterrath, T., Brendel, C., Hafer, M., Junghänel, T., Klameth, A., Lengfeld, K., Walawender, E., Weigl, E., and Becker, A.: RADKLIM Version 2017.002: Reprozessierte, mit Stationsdaten angeeichte Radarmessungen (RADOLAN), 5-Minuten-Niederschlagsraten (YW), [https://doi.org/10.5676/DWD/RADKLIM\\_YW\\_V2017.002](https://doi.org/10.5676/DWD/RADKLIM_YW_V2017.002), 2018.

1330 Woollings, T., Barriopedro, D., Methven, J., Son, S.-W., Martius, O., Harvey, B., Sillmann, J., Lupo, A. R., and Seneviratne, S.: Blocking and its response to climate change, *Curr. Clim. Change Rep.*, 4, 287–300, <https://doi.org/10.1007/s40641-018-0108-z>, 2018.

Zhang, C., Wang, Y., and Hamilton, K.: Improved Representation of Boundary Layer Clouds over the Southeast Pacific in ARW-WRF Using a Modified Tiedtke Cumulus Parameterization Scheme, *Mon. Weather Rev.*, 139, <https://doi.org/10.1175/MWR-D-10-05091.1>, 2011.

Zhang, F., Sun, Y. Q., Magnusson, L., Buizza, R., Lin, S.-J., Chen, J.-H., and Emanuel, K.: What is the predictability limit of midlatitude

1335 weather?, *J. Atmos. Sci.*, 76, 1077–1091, <https://doi.org/10.1175/JAS-D-18-0269.1>, 2019.

# Supplementary Material

## A Data and Methods

### Heavy precipitation statistics: KOSTRA

KOSTRA (*Koordinierte Starkniederschlagsregionalisierung und -auswertung*; latest version KOSTRA-DWD-2010R; Malitz 1340 and Ertel, 2015; Junghänel et al., 2017) is a gridded data set of roughly  $8 \times 8 \text{ km}^2$  horizontal resolution containing precipitation statistics for Germany provided by the German Weather Service (DWD). It is based on ground-based observational station data interpolated to the regular grid for duration levels below 24 hours and on HYRAS-DE for longer intervals. KOSTRA provides statistics on different duration levels ranging from 5 minutes to 72 hours and return periods between 1 year and 100 years. It is widely used in Germany for precipitation–runoff estimations and the dimensioning of facilities.

1345

### Antecedent Precipitation Index

As mentioned in [PART1](#)[PART 1](#), antecedent wetness conditions can be an important driver for the precipitation–runoff response in a river basin. An established quantity to describe the preconditions is the Antecedent Precipitation Index (API; e.g., Kohler 1350 and Linsley, 1951; Viessman et al., 2002). API is a weighted summation over  $N$  days prior to the event day using a weighting factor  $k$ . In line with [PART1](#)[PART 1](#) and previous studies (e.g., Heggen, 2001; Schröter et al., 2015), we use  $N = 30$  days and  $k = 0.9$ . For [PART2](#)[PART 2](#), API is applied to the daily HYRAS-DE data set. For the statistical analyses, a normalized version [NAPI](#)[of API \(NAPI\)](#) is defined as follows:

$$\text{NAPI} = \frac{\text{API}(x, y, t)}{\text{cAPI}(x, y, d)} - 1, \quad (1)$$

where  $(x, y)$  denotes the grid point position,  $t$  is the day of interest, and  $d$  is the corresponding calendar day of  $t$  between 1355 1 January and 31 December. cAPI is the climatological mean over the entire time series of HYRAS-DE on the corresponding calendar day  $d$ . By subtracting 1, NAPI is centered around zero, meaning that negative values describe drier conditions and positive values [are](#) wetter conditions than the climatology.

### High resolution climate model simulations: KIT-KLIWA

1360

**Table S1.** Driving GCMs of the KIT-KLIWA CPM simulations with related references and used realization, and the 30-year time periods that corresponds to the global warming level of +2 °C (GWL2) and +3 °C (GWL3) based on the method of Teichmann et al. (2018).

GCM	Reference	Realization	GWL2	GWL3
MPI-ESM-LR	Giorgetta et al. (2013)	r1i1p1	2029–2058	2052–2081
EC-EARTH	Prodhomme et al. (2016)	r12i1p1	2026–2058	2051–2080
CNRM-CM5	Volodire et al. (2013)	r1i1p1	2029–2058	2052–2081
HadGEM2-ES	Collins et al. (2011)	r1i1p1	2016–2045	2037–2066

## B Classification in the historical context

**Table S2.** Heaviest precipitation events in Germany between 1951 and 2021 based on daily HYRAS-DE and fulfilling the empirical heavy precipitation event criterion  $HPE_{crit}$  (sorted in descending order regarding the area  $A$ ,  $rk_{HPEcrit}$ ; see Sect. 2.3.2). The events are the same as shown in excerpts in Figures 2, 223, 4, and S1.  $A$  represents the contiguous area of HYRAS-DE grid cells exceeding the 50-year return level of KOSTRA. Given are the mean precipitation amount  $\bar{R}$  averaged over  $A$ , the maximum grid point precipitation  $R_{max}$  within  $A$ , the API value averaged over  $A$  and its deviation from the corresponding climatology NAPI, the PSI-value, the rank according to the PSI rk<sub>PSI</sub>, the maximum return interval-period of areal precipitation  $T_{max}$  regarding LAERTES-EU and related area  $A_{T_{max}}$  at which  $T_{max}$  is reached (derived from Fig. 5). **Bold numbers** represent the maximum of the corresponding column, except for  $A_{T_{max}}$  as a range is given in this case.

$rk_{HPEcrit}$	Date	$A$ (km $^2$ )	$\bar{R}$ (mm)	$R_{max}$ (mm)	$\bar{API}$ (mm)	NAPI	$PSI rk_{PSI}$	$T_{max}$ (a)	$A_{T_{max}}$ (km $^2$ )
1	8 Aug. 1978	<b>20 851</b>	124.6	183.9	17.63	0.13	<b>2.40</b> <del>1</del> > 1000	7000–20 000	
2	17 Jul. 2002	13 099	91.5	152.0	34.47	0.87	<b>2.20</b> <del>2</del> 100	30 000–40 000	
3	12 Aug. 2002	10 826	<b>138.8</b>	<b>262.0</b>	50.03	1.78	<b>1.68</b> <del>5</del> > 1000	500–1000	
4	29 Jun. 2017	10 225	91.2	175.2	25.69	0.81	<b>1.70</b> <del>4</del> 20	10 000–20 000	
5	14 Jul. 2021	8354	100.2	154.3	62.90	1.59	<b>0.80</b> <del>23</del> 50	15 000–20 000	
6	26 Aug. 2010	7151	113.6	153.8	46.08	1.32	<b>4.02</b> <del>18</del> 50	6000–8000	
7	29 Jun. 1981	7017	93.0	138.8	36.78	0.74	<b>4.22</b> <del>15</del> 20	12 000–25 000	
8	18 Jul. 1987	6750	110.3	141.4	29.55	1.42	<b>4.47</b> <del>7</del> 20	3000–5000	
9	8 Jul. 1954	6616	109.6	212.9	91.51	3.40	<b>4.11</b> <del>17</del> 50	3000–5000	
10	30 Jun. 2021	3943	137.7	192.0	7.50	-0.44	<b>4.56</b> <del>6</del> 100	1000–1500	
11	27 Aug. 1989	3876	81.3	96.5	20.74	0.05	<b>4.14</b> <del>16</del> 10	15 000–20 000	
12	9 Jul. 2021	3676	70.2	78.8	13.29	-0.21	<b>4.25</b> <del>13</del> 1	50 000–60 000	
13	22 Jul. 2011	2740	80.7	105.6	56.03	2.84	<b>0.96</b> <del>20</del> < 1	–	
14	29 Aug. 1969	2139	92.5	121.3	21.26	0.52	<b>4.35</b> <del>11</del> 10	7000–10 000	
15	21 May 1999	1738	134.6	196.2	84.77	3.19	<b>0.74</b> <del>25</del> 50	2000–3000	
	12 Jun. 1993	1738	81.7	114.4	38.73	1.44	<b>4.01</b> <del>19</del> 10	20 000–30 000	
17	4 Aug. 1983	1671	92.9	107.8	19.71	0.27	<b>4.43</b> <del>8</del> 5	5000–15 000	
	27 Sep. 1965	1671	83.7	97.9	13.46	-0.37	<b>0.77</b> <del>24</del> 1	5000–15 000	
19	16 Jul. 1965	1470	99.2	130.9	82.40	3.13	<b>4.23</b> <del>14</del> 2	8000–15 000	
	28 Jul. 2000	1470	86.5	100.7	29.52	0.96	<b>0.94</b> <del>21</del> 2	3000–5000	
21	15 Jul. 1956	1136	96.2	119.1	36.73	1.49	<b>4.42</b> <del>9</del> 5	15 000–50 000	
	27 Oct. 1998	1136	74.1	85.6	52.86	1.71	<b>4.36</b> <del>10</del> 2	6000–80 000	
23	9 Jul. 1954	1069	102.0	133.3	<b>110.15</b>	<b>5.30</b>	<b>4.76</b> <del>3</del> 10	20 000–50 000	
24	18 Jul. 2002	1002	97.4	124.4	80.62	2.96	<b>4.27</b> <del>12</del> 1	1000–2000	
	1 Jun. 2016	1002	87.7	118.2	45.44	1.32	<b>0.84</b> <del>22</del> 1	1000–2000	
	4 Sep. 1995	1002	85.2	108.6	28.73	0.18	<b>0.42</b> <del>26</del> < 1	–	

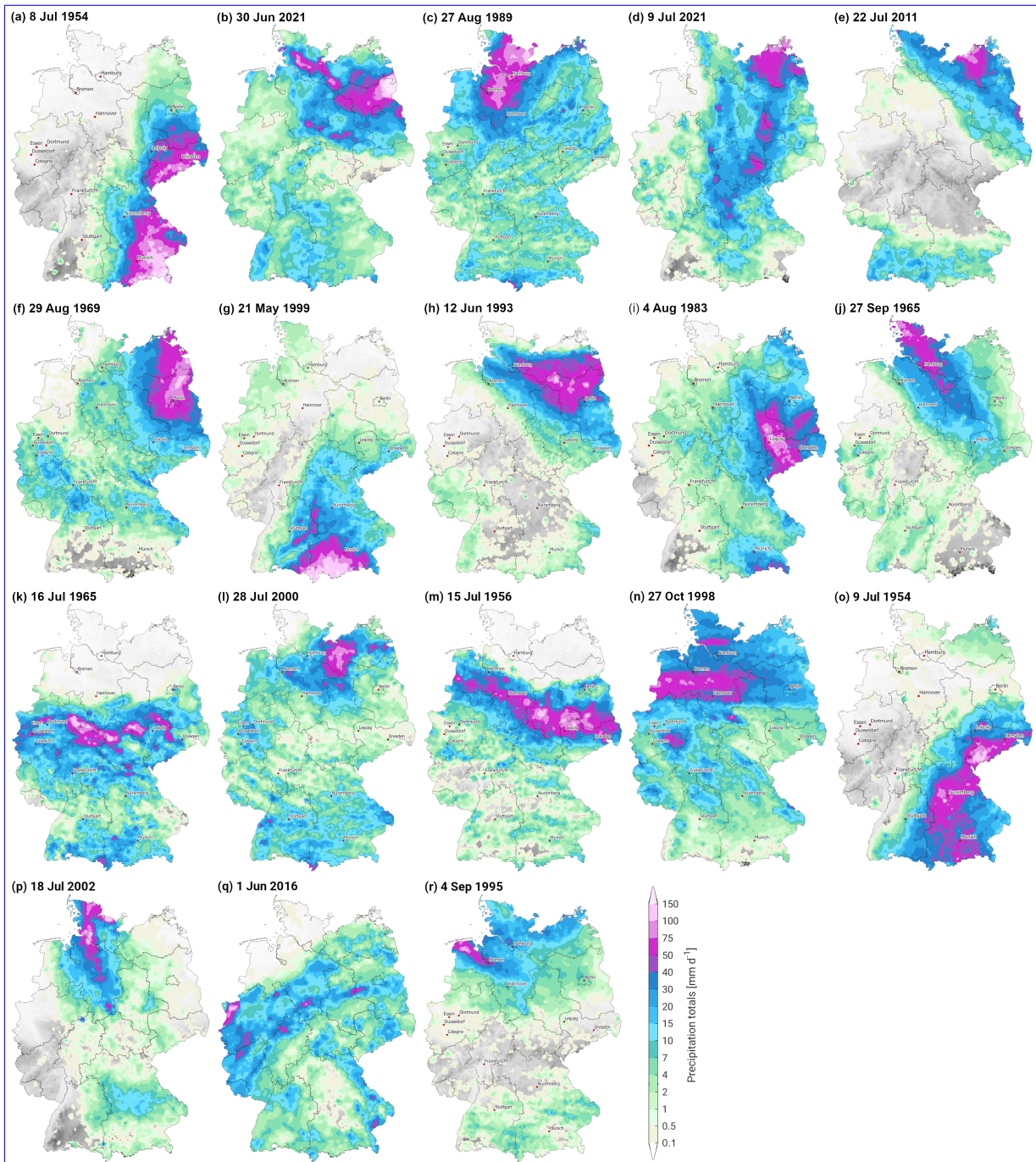


**Figure S1.** Same as Fig. 2, but for the heavy precipitation events in Germany ranked 9th (a) to 20th (r) according to the  $\text{HPE}_{\text{crit}}$  criterion (based on daily HYRAS-DE data, 1951 to 2021). See also Table S2 with further statistics.

## C Relation to climate change

**Table S3.** Relative increase of daily precipitation  $\Delta$  (in % per degree global warming) for different return periods (RP) calculated from the reference period (1971 to 2000) to GWL2 and from the reference period to GWL3. The Given are the mean was (mn) and the 25th (p25) and 75th (p75) percentile calculated over all ensemble members and all grid points within CReg or LReg, respectively.

RP (in a)	$\Delta_{\text{CReg}}$ (in %)						$\Delta_{\text{LReg}}$ (in %)					
	GWL2			GWL3			GWL2			GWL3		
	p25	mn	p75	p25	mn	p75	p25	mn	p75	p25	mn	p75
1	2.9	6.2	9.1	2.8	5.6	8.0	2.6	6.3	9.4	3.0	5.4	7.5
3	2.5	7.3	11.6	3.2	6.8	10.0	2.5	7.5	11.7	3.3	6.5	9.2
5	2.0	7.9	13.0	3.2	7.5	11.2	2.3	8.1	13.0	3.3	7.0	10.2
10	1.2	8.8	15.2	3.0	8.4	12.9	1.8	9.0	15.0	3.1	7.8	11.7
30	-0.5	10.3	19.1	2.5	10.1	16.2	0.9	10.7	18.6	2.8	9.2	14.4